POINT FOCUSING X-RAY MONOCHROMATOR
FOR
LOW ANGLE SCATTERING STUDIES

Thesis by

Leon Shenfil

In Partial Fulfillment of the Requirements

For the Degree of

Doctor of Philosphy

California Institute of Technology

Pasadena, California

~~1952~~
1952

ACKNOWLEDGEMENTS

I wish to take this opportunity to thank Professor Jesse W. M. DuMond for suggesting this thesis project and for taking a keen interest in the course of its development. His helpful suggestions have been instrumental in the success of this work. In the three years that I have worked for him as a graduate student, I have profited considerably from his vast experience and have learned a good deal of the practical side of physics, the sort of thing one does not find in text-books. For this, I wish to express my deepest gratitude.

To Warren E. Danielson, who shares equally in the design and construction of the point focusing monochromator, I wish to extend my hearty thanks and the hope that he will find many interesting applications of the instrument.

This project was supported jointly by the Office of Naval Research and the Atomic Energy Commission.

ABSTRACT

A point focusing x-ray monochromator was designed and constructed for low angle scattering studies. The anastigmatic point focus is achieved by means of two cylindrically bent quartz crystals whose focal circles are mutually perpendicular. The beam, emanating from the copper target of an x-ray tube, is reflected in succession, first from the crystal defining the horizontal focal circle and, second from the crystal defining the vertical focal circle following which it comes to a monochromatic point focus of wavelength 1.537 Å (Cu $K\alpha_1$). The sample to be studied is placed between the second crystal and the point focus, and the scattered beam is detected by means of a photographic plate placed at the point focus, at right angles to the undeviated beam, the latter being suppressed by means of an absorber.

Mathematical analysis, in which a ray was traced through the two crystal system, revealed correctly the shape and size of the point focus, and the possibility of reducing the latter in size by stopping down the beam emerging from the target.

The instrument and its lining up procedure is described in detail, particularly the latter since the orientation of the two crystals relative to each other and the x-ray tube involve twelve degrees of freedom.

Suggestions for improving the intensity of the instrument are made. These consist of (1) substitution of topaz crystals for quartz, (2) use of helium atmosphere instead of air to surround the x-ray beam (3) reorientation of the x-ray tube to permit smaller angles of emergence of the beam.

As a trial run for the instrument, the scattering patterns of two kinds of carbon black (good scatterers) were obtained from which the average particle sizes and size distributions were calculated.

TABLE OF CONTENTS

PART I

INTRODUCTION

In the past few years a good deal of interest has arisen in low angle x-ray diffraction studies, particularly among chemists and biologists. It is well known[1] that x-rays scattered at low angles reveal the size, and possibly the shape of small particles that make up the scatterer. In the case of fibrous substances, such studies[2] may reveal the size of large periodicities along the fibers. In a way, one can think of low angle studies as being an extension of microscopy into smaller sizes although the "pictures" that one obtains are by no means as easy to interpret. In the case of particles, the intensity, in general, is a function of $\epsilon r/\lambda$ where ϵ is the scattering angle, r the particle radius and λ the x-ray wavelength being scattered.[1,3] Theoretical curves of intensity versus scattering angle have been computed for particles of various sizes, shapes and size distributions[4], so that all one has to do is to match the intensity distribution of the scattered x-rays with one of the theoretical curves in order to determine the physical properties of the scatterer. This seemingly simple procedure, however, is complicated by several factors. The intensity distribution that one obtains in practice is the fold (or convolution) of the spectral distribution of the x-rays, the beam aperture, and the scattering distribution, thus posing the problem of separating or unfolding the first two factors in order to obtain the actual scattering distribution. The problem of unfolding is a very difficult one

particularly if one doesn't know exactly what functions formed the fold in the first place.

Thus, to obtain a scattering pattern which is truly representative of the scattering medium, one has to try to minimize the instrumental effects, by constructing an instrument which will produce a monochromatic beam of high spectral resolution. However, as is usually the case, the price of high resolution is loss of intensity which in many cases is so serious as to defeat the whole purpose of the experiment. Various types of instruments have been built in the past in which a compromise, of some form or another, has been made between high resolution and low intensity. These instruments can be classed roughly into two types: (1) the slit type instrument consisting of an x-ray beam, possibly filtered, which is collimated by a slit system or (2) the crystal type, in which one or two crystals (either flat or bent) are used to monochromatize the beam.

The slit type instrument is best adapted for long wavelengths, thus requiring vacuum methods. This is a handicap which is shared by an electron microscope, especially when scattering from liquid samples is desired. Successful use of such an instrument has been reported by Yudowitch[5], and Bolduan and Bear[2,6].

An instrument for low angle scattering studies in which a curved crystal is used for monochromatization has been reported by Guinier[1] and later at the suggestion of DuMond,

has been modified by the addition of a second curved crystal placed in the "parallel"* position with respect to the first.** See Fig. 1. In the latter scheme, the sample is placed in the convergent beam, midway between the second crystal and the line focus, while the photographic plate is placed in the focal plane. The diffraction pattern appears on the photographic plate as a diffuse distribution symmetrically disposed on either side of the direct beam, the latter being suppressed by means of an absorber. It has been found that line focused beams are not well adapted in the study of the long chains of protein molecules in which the periodicities of interest are along the chain.

The possibility of bringing a monochromatic beam of x-rays to an anastigmatic point focus was first suggested by DuMond in 1949(7), however, due to lack of funds the design and construction of a point focusing instrument were not undertaken until the summer of 1950.

---

*The "parallel" position is the position of zero dispersion. See Compton and Allison(8), p. 718, where the term is used in relation to two flat crystals.

**The beam is focused monochromatically to a line by reflection from the first crystal and is refocused again to a line by reflection from the second crystal, thus cutting down the incoherent scattering in the neighborhood of the line focus. This is not to be confused with the instrument whose development forms the subject matter of the present thesis in which the angles of deviation of the beam in the two successive crystal reflections lie in planes at right angles to each other in such a way that the beam is brought to an anastigmatic point focus.

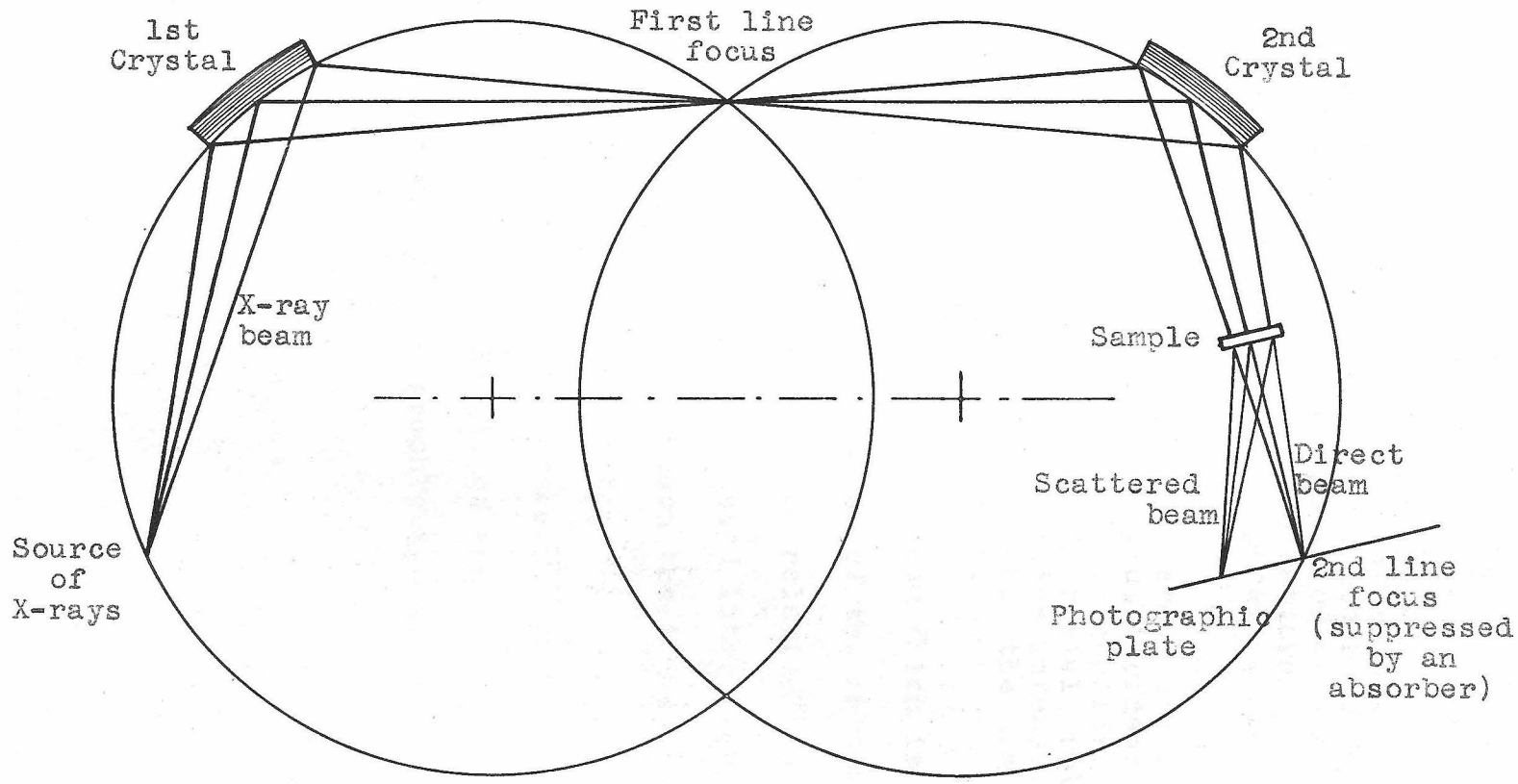

Fig. 1 - Two crystal line focusing monochromator.

The advantages of a point focusing monochromator are two-fold:

1. The circular symmetry of the scattered radiation greatly simplifies the interpretation of intensity distributions. In other words, the point focused beam may be thought of as such a fine tool that any diffraction pattern obtained with it must be considered as purely a property of the scatterer.*

2. The background due to incoherent scattering of the continuous x-ray spectrum incident on the first crystal will be reduced considerably after scattering from the second crystal, relative to the twice Bragg reflected line intensity, thus improving the sensitivity when the scattering power of the sample is weak.

The intensity of the focused beam which is discussed in some detail later, is probably one of the factors that may limit the use of the instrument to relatively good scatterers. Several improvements, also discussed later, may increase the luminosity considerably. Although the intensity (power/unit area) of the beam at the point focus is considerable, the actual power in the beam is not sufficiently high at present to permit measurable diffusion of the beam by a scatterer over a large area of photographic plate.

---

*The size of the point can be decreased at will by stopping down the beam emerging from the target. Without such stops and with our present x-ray tube (Machlett), the point appears slightly elongated with dimensions 0.196 by 1.40 mm.

PART II

GEOMETRY OF THE POINT FOCUSING MONOCHROMATOR

Since the point focusing monochromator consists of two bent crystals, each of which behaves like a line focusing monochromator, it will be well to review briefly the geometry of a single bent crystal. The numerous symbols used in the discussion that follows are listed alphabetically at the end of this part (p. 39).

GEOMETRY OF A SINGLE BENT CRYSTAL

It is well known[9] that x-rays can be made to focus monochromatically by a crystal lamina which has been hollowed out, cylindrically, to a given radius and then bent elastically to half that radius. If we let the concave face of the crystal after bending define a cylinder, then the intersection of this cylinder with a plane, bisecting the crystal and perpendicular to the generators, is a circle called the focal circle. The plane is called the focal plane. The only condition required for point focusing is that the line, about which the crystal planes are concentric, be one of the generators of the focal cylinder.

Fig. 2 shows a single crystal with its focal circle. C is the center of the circle, S a point-source of x-rays, F the vertical line focus, P some arbitrary point on the crystal, and β the vertical line about which the crystal planes are concentric. Thus, the figure shows the projection of the rays $\overline{SP}$ and $\overline{PF}$ on the focal plane with $\overline{\beta P}$ normal to the crystal

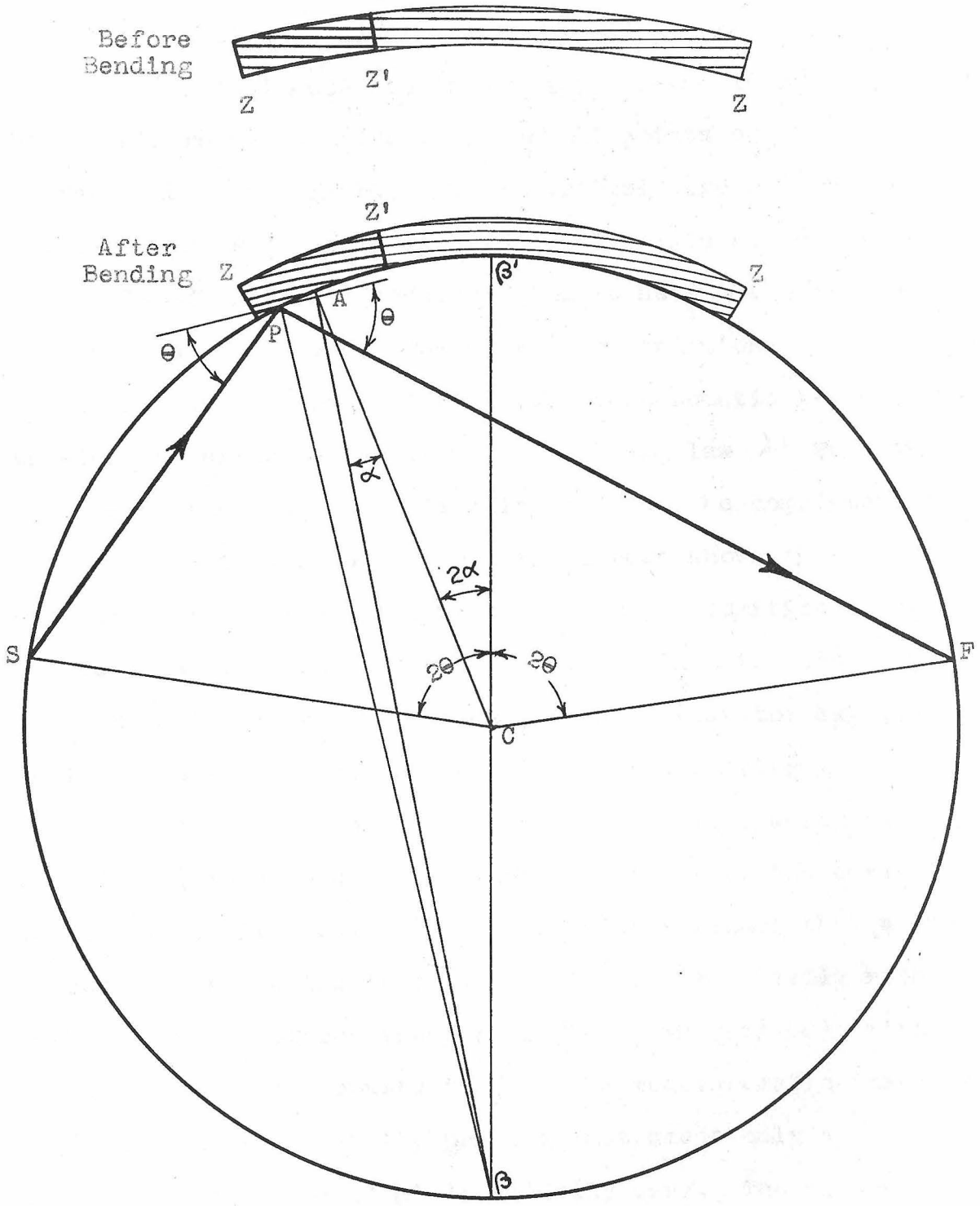

Fig. 2 - Geometry of a single bent crystal, cylindrically ground before bending.

planes at P. ($\overline{SP}$ and $\overline{PF}$ are in a plane not necessarily parallel to the focal plane.) If the arcs $\widehat{S\beta}$ and $\widehat{\beta F}$ are equal, then the angle of incidence $\widehat{SP\beta}$ is equal to the angle of reflection $\widehat{\beta PF}$. This relation holds true for all points on the crystal surface and, furthermore, if the vertical divergence (angle between rays $\overline{SP}$ or $\overline{PF}$ and the focal plane) is not excessive, the angle of incidence remains fairly constant for all points on the crystal surface. The above two conditions are precisely the ones required for reflection of monochromatic x-rays. The wavelength reflected is given by the Bragg law $\lambda = 2d \sin\theta$ where θ is the grazing angle which is also the complement of the angle of incidence. Thus, it has been shown that a beam emanating from the point S will focus monochromatically at the vertical line through F. Experimentally, the position of point S, relative to the crystal, is such that the $K\alpha_1$ line of Cu is reflected in the monochromator here described.

In Fig. 2, the point on the focal circle diametrically opposite β, is denoted by β', and the center of the crystal lamina by A. It should be clear from this figure that a much larger crystal lamina (such as that indicated, partly with lighter lines, between the points ZZ in the figure), with center at β' could be used to form the monochromatic image at F of the source S. In the present instrument only a portion ZZ' entirely on one side of β' is actually used. The reason why the center of the crystal is not at β', but to the left of it, will be evident as soon as the two-crystal arrangement is

discussed.

The angle 2α is a measure of the angular displacement of point A from β'. Since the angle $\widehat{\beta AC}$ is equal to α, then α is also the dihedral angle between the crystal plane and its face (or between their normals) at the point A and at all points lying on the generator through A.

The reflected beam that arrives at F appears to come from the virtual line source F' which lies on a circle of radius $S\beta'$ with β' as center, see Fig. 3. Now let us take a second identical crystal with its focal plane perpendicular to the focal plane of the first crystal and place it in such a way that the line of intersection of the two focal planes is FF'. Let the center of the second crystal be denoted by B, then both B and A are on the line FF'. If we let BF' = AF and if the point F' lies on the focal circle of the second crystal, then the rays striking this crystal will be reflected at the Bragg angle and will come to a point focus, P.F.

It should now be evident, (1) why only a <u>part</u> , ZZ', of the total conceivable crystal ZZ shown in Fig. 2 is retained, (2) why the center A of the crystal ZZ' is displaced angularly by an amount 2α from the point β' and (3) why the atomic reflecting planes of the crystal are not exactly parallel to the face of the bent crystal slab at its center but make an angle α therewith. All three of these requirements originate from the fact that the first crystal must be kept entirely on one side of the point β' and the second crystal entirely on

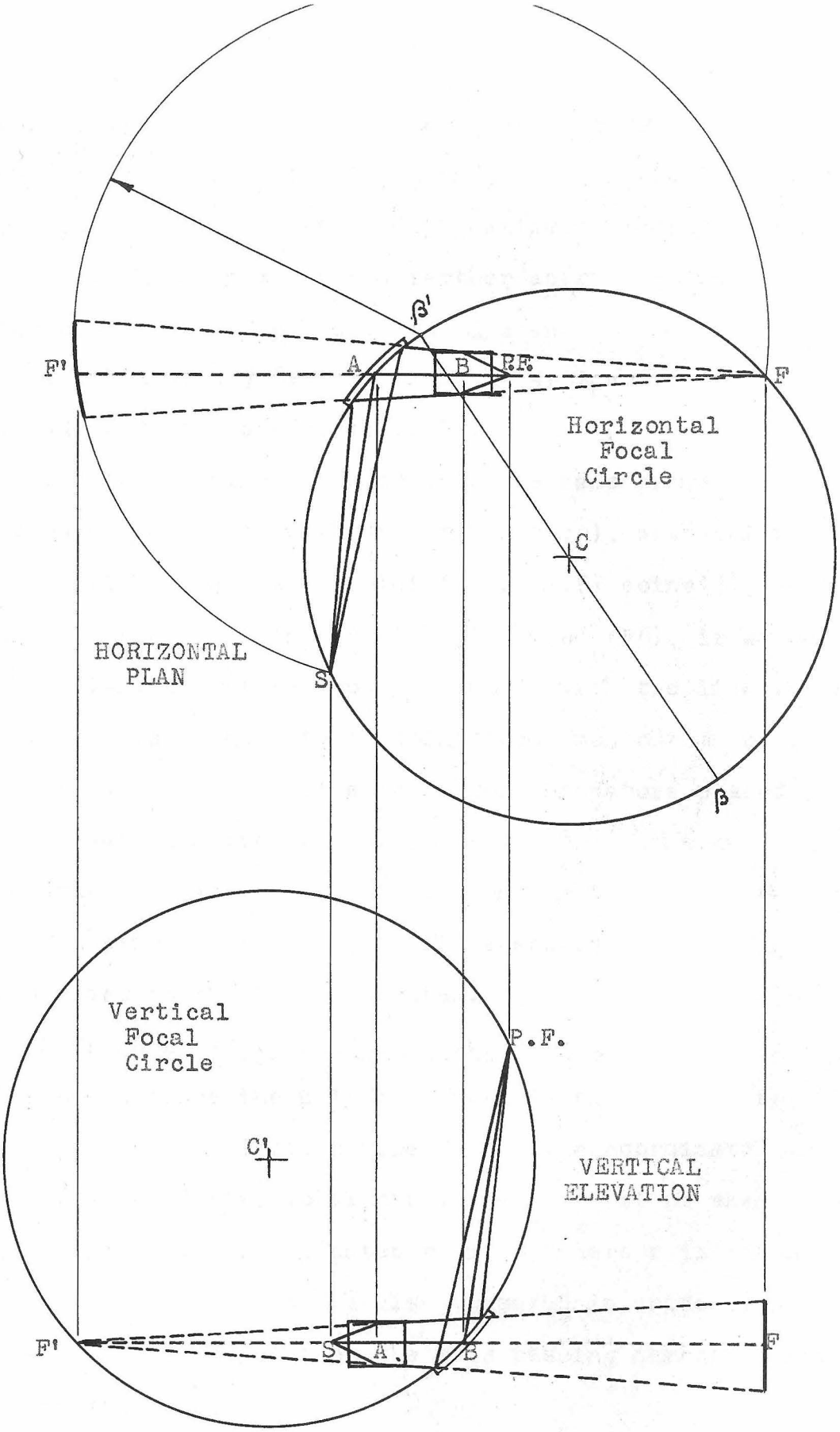

Fig. 3 - Two bent crystals arranged to form a point focusing monochromator.

the other side so as to avoid interference between the two crystals or their crystal holders when the two focal circles are correctly mounted to avoid astigmatism. Clearly, the larger the angle α is made, the farther apart the two crystal clamping blocks may be placed. The distance between the centers A and B of the two crystals is given by $4r\sin\alpha\cos\theta$ where r is the radius of either focal circle.

If the two focal circles were in the same plane and superimposed on one another (without turning over), with point B coinciding with A, and with point focus (P.F) coinciding with the point source (S) then the virtual source (F'), if we neglect the slight curvature, would coincide with the line focus (F). It is thus seen that the point focus monochromator is made up of two identical line focus monochromators placed in a definite way relative to one another.

In order to examine the aberrations that occur in such a point focusing arrangement, it is necessary to take a general ray and trace it through the system.

TRACING A GENERAL RAY THROUGH THE SYSTEM

For convenience the unit of length is taken equal to the radius of one of the focal circles. Let the coordinates describing the horizontal focal circle be x, y, z, or when convenient, cylindrical coordinates ρ, ϕ, z, where z is perpendicular to the focal plane and is also measured in units of r and ρ is the radial distance from the axis passing through C normal to the focal circle.

In Fig. 4, S_o represents the center of the target which is on the focal circle, S the intersection of a beam from an arbitrary point on the target with the focal cylinder*, A the center of the crystal, P some arbitrary point on the crystal with coordinates (l, ϕ, z), F_o the focal point, and β the vertical axis about which the crystal planes are concentric. The x-axis is in the focal plane, perpendicular to $\overline{AF_o}$. In the calculations that follow, we will derive the relation between the grazing angle θ, defined on p. 15 and the Bragg angle θ_o, defined below.

$\overline{S_oP}$ represents a ray of wavelength λ_o such that the angle θ_o satisfies the Bragg law $\lambda_o = 2d \sin \theta_o$. λ_o is the wavelength at the middle of the $K_{\alpha 1}$ line.

The angle between the projection of $\overline{S_oP}$ on the xy plane and the x-axis is $-(\frac{\pi}{2} - \frac{3\theta_o - \alpha + \phi}{2})$.** The length of $\overline{S_oP}$ is

$$|\overline{S_oP}| = \left[4\sin^2\left(\frac{3\theta_o - \alpha - \phi}{2}\right) + z^2\right]^{\frac{1}{2}}$$

$$= 2\sin\frac{3\theta_o - \alpha - \phi}{2}\left[1 + z^2/\left(4\sin^2\frac{3\theta_o - \alpha - \phi}{2}\right)\right]^{\frac{1}{2}}$$

and the length of its projection on the xy plane is

$$2\sin\frac{3\theta_o - \alpha - \phi}{2}$$

---

*The plane of the target is not tangent to the focal cylinder. It is oriented in such a way that the central ray $\overline{S_oA}$ makes approximately 6° with it. This direction of $\overline{S_oA}$ is the direction of maximum intensity.

**The angle α has the same significance explained for Fig. 2 and the angle ϕ in Fig. 4, is the angle $\widehat{PCX}$.

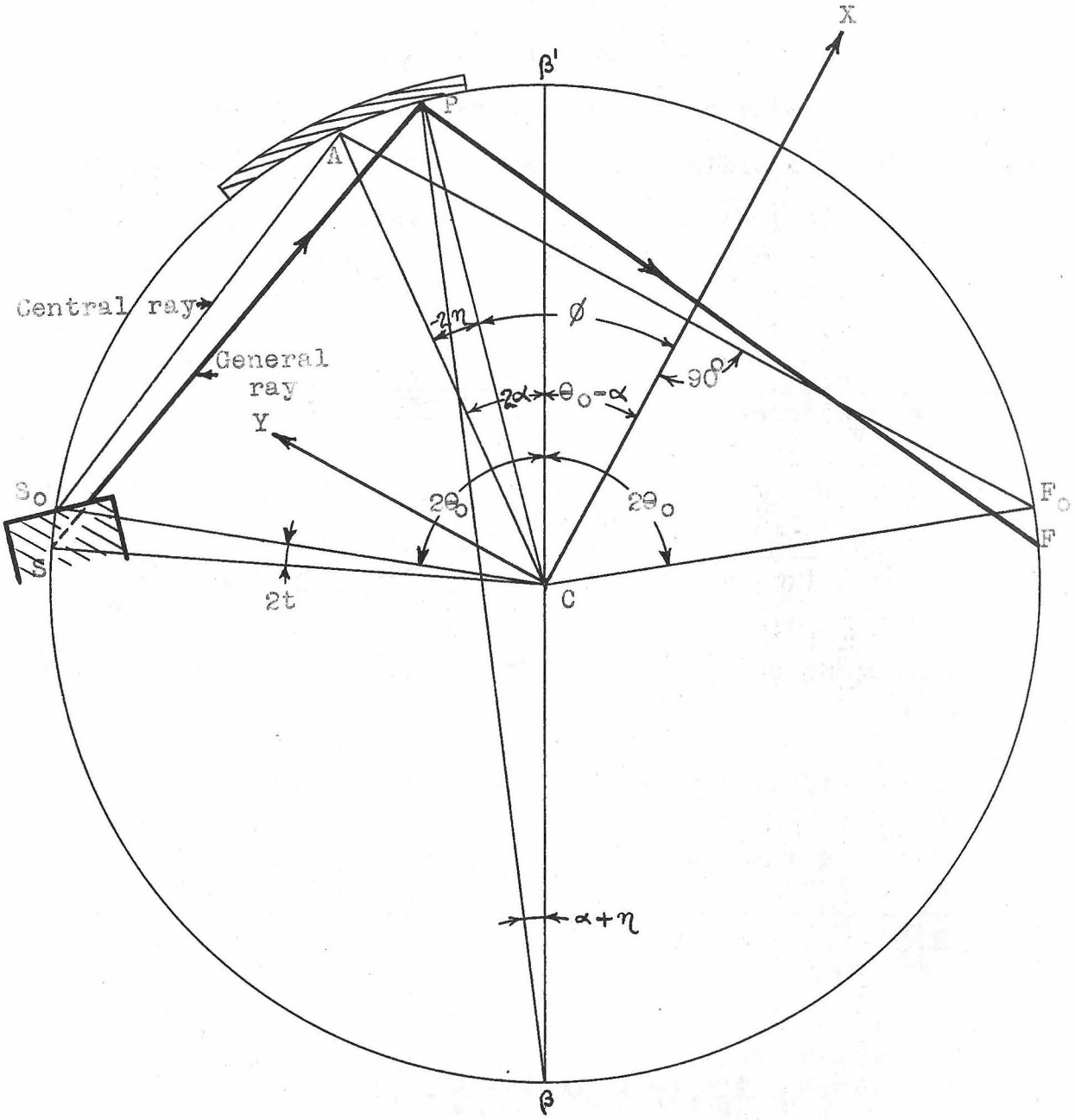

Fig. 4 - Horizontal focal circle shown with its coordinate axes.

It will be convenient to measure angles from $\overline{AC}$ rather than the x-axis. We therefore define the central angle $\widehat{ACP}$ by 2η and from Fig. 4 it is seen that,

$$2\eta = \phi - \theta_o - \alpha \tag{1}$$

Because of the limited size of the crystal, η will never exceed 1/80 radians. This makes it possible to neglect terms of order η^3, since they represent angles that are smaller than one second of arc.*

Let,

$$a_o = \left[1 + \frac{z^2}{4\sin^2 \frac{3\theta_o - \alpha - \phi}{2}}\right]^{\frac{1}{2}} = \left[1 + \frac{z2}{4\sin^2(\theta_o - \alpha - \eta)}\right]^{\frac{1}{2}}$$

and

$$b_o = \frac{z}{2\sin \frac{3\theta_o - \alpha - \phi}{2}} = \frac{z}{2\sin(\theta_o - \alpha - \eta)}$$

This gives $\overline{S_oP} = za_o/b_o$ and the length of its projection on the xy plane is z/b_o.

The direction cosines of $\overline{S_oP}$ are therefore:

$$\frac{\frac{z}{b_o}\cos(\frac{\pi}{2} - \frac{3\theta_o - \alpha + \phi}{2})}{\frac{za_o}{b_o}}, \frac{-\frac{z}{b_o}\sin(\frac{\pi}{2} - \frac{3\theta_o - \alpha + \phi}{2})}{\frac{za_o}{b_o}}, \frac{\frac{z}{za_o}}{\frac{b_o}{b_o}}$$

or by substituting (1)

$$\frac{1}{a_o}\sin(2\theta_o + \eta), -\frac{1}{a_o}\cos(2\theta_o + \eta), \frac{b_o}{a_o} \tag{2}$$

---

*The half-width at half maximum of the Darwin diffraction pattern for $K\alpha_1$ radiation of copper reflected from quartz in the 1st order of the (310) planes is about 1 second of arc and this, therefore, has been taken as the limit of negligibility.

The above ray is emitted from the point S_o whose coordinates are $(1, 3\theta_o - \alpha, 0)$. Suppose now, a ray is emitted from the neighborhood of S_o, say the point S, whose coordinates relative to S_o are (t_y, t_z), see Fig. 5, or relative to the focal circle $(1, 3\theta_o - \alpha + 2t, t_z)$ where $t = ty/2\sin(\theta_o - \alpha)$, then the direction cosines of $\overline{SP}$ follow from (2)

$$\frac{1}{a} \sin(2\theta_o + \eta + t), \frac{1}{a} \cos(2\theta_o + \eta + t), \frac{b}{a} \tag{3}$$

where

$$a = \left[1 + \frac{(z - t_z)^2}{4 \sin^2(\theta_o - \alpha - \eta + t)}\right]^{\frac{1}{2}} \tag{4}$$

and

$$b = \frac{z - t_z}{2 \sin(\theta_o - \alpha - \eta + t)} \tag{5}$$

The projected target size is 1 mm. x 1 mm. at right angles to the central ray so that $|t| = |ty/2\sin(\theta_o - \alpha)| \leq 1/1500$ radians and $|t_z| \leq 1/1200$ radians.

$\overline{P\beta}$ represents the normal to the crystal planes at point P and its direction cosines are:

$$\cos \frac{\phi + \theta_o - \alpha}{2}, \sin \frac{\phi + \theta_o - \alpha}{2}, 0$$

or by substitution of (1)

$$\cos (\theta_o + \eta), \sin (\theta_o + \eta), 0 \tag{6}$$

Now let θ be the grazing angle of the ray at point P, i.e. the angle that the ray makes with the crystal planes, so

that $\frac{\pi}{2} - \theta$ is the angle between $\overline{SP}$ and $\overline{P\beta}$, then

$$\cos\left(\frac{\pi}{2} - \theta\right) = \sin\theta = \frac{\overline{SP} \cdot \overline{P\beta}}{|\overline{SP}|\,|\overline{P\beta}|}$$

With the help of (3) and (6), this gives

$$\sin\theta = (1/a)\left[\sin(2\theta_o + \eta + t)\cos(\theta_o + \eta) - \cos(2\theta + \eta + t)\sin(\theta_o + \eta)\right]$$

or

$$\sin\theta = (1/a)\,\sin(\theta_o + t) \tag{7}$$

From (4) and (5), $a = (1 + b^2)^{\frac{1}{2}}$, where b^2 is small, so that terms of order b^4 in the expansion of $1/a$ can be neglected. Therefore,

$$1/a \approx 1 - b^2/2 \tag{8}$$

and,

$$\sin\theta \approx \sin(\theta_o + t) - (b^2/2)\,\sin(\theta_o + t)$$

The second term on the right represents a small correction to the angle θ, which can be expressed as follows:

$$\theta = \theta_o + t - \gamma \tag{9}$$

$$\sin\theta = \sin(\theta_o + t - \gamma) \approx \sin(\theta_o + t) - \gamma\cos(\theta_o + t)$$

γ is identified by comparing with the preceding equation, and is given by

$$\gamma = \frac{b^2}{2}\,\tan(\theta_o + t) \tag{10}$$

or upon elimination of b with equation (5), by

$$\gamma = \frac{(z - t_z)^2\,\tan(\theta_o + t)}{8\,\sin^2(\theta_o - \alpha - \eta + t)} \approx \frac{z^2\,\tan\theta_o}{8\,\sin^2(\theta_o - \alpha)} \tag{10a}$$

Also, since z is at most 1/60 radians and the arguments of the tangent and sine are approximately $\pi/4$ so that $\gamma \approx 15$ sec. of

arc, it was therefore justifiable to omit terms of order b^4 in eq. (8).

We have thus obtained an expression for the grazing angle θ of a ray of wavelength λ_o, from the point S, in terms of the Bragg angle θ_o and the small angular deviations t and γ.

It is now necessary to consider wavelengths that are slightly different from λ_o, since the whole $K_{\alpha 1}$ line contributes to the beam rather than just a small portion of it represented by λ_o. Let the new wavelength be λ and the Bragg angle corresponding to it θ_B, then because of the smallness of $\lambda - \lambda_o$, it is possible to expand θ_B in a power series, keeping only two terms, thus:

$$\theta_B = \theta_o + (\lambda - \lambda_o) \frac{\partial \theta_o}{\partial \lambda} \tag{11}$$

where

$$\frac{\partial \theta_o}{\partial \lambda} = \frac{1}{2d \cos \theta_o} = \frac{\tan \theta_o}{\lambda_o}$$

obtained by differentiating the Bragg equation $\lambda_o = 2d \sin\theta_o$.

The intensity reflected by the crystal is a function of the difference between the grazing angle and the Bragg angle. Subtracting (11) from (9), we get

$$\theta - \theta_B = t - \gamma - (\lambda - \lambda_o) \frac{\partial \theta_o}{\partial \lambda} \tag{12}$$

or upon replacing γ and $\frac{\partial \theta_o}{\partial \lambda}$ by their equivalent expressions

$$\theta - \theta_B = t - \frac{z^2 \tan\theta_o}{8 \sin^2(\theta_o - \alpha)} - \frac{\lambda - \lambda_o}{\lambda_o} \tan\theta_o \tag{12a}$$

The intensity of the diffraction pattern of the crystal can be written as $F_{\substack{\sigma \\ \pi}} = F_{\substack{\sigma \\ \pi}}(\theta - \theta_B)$* and its shape in the case of no absorption is given by Compton and Allison[8], Fig. VI-7. The full width at half maximum of the diffraction pattern, in the case of the (310) planes of quartz, is approximately 2 seconds of arc. This means that for $\theta - \theta_B > 1''$ only a small fraction of the intensity of wavelength λ is reflected. In the preceding calculations angles that are less than the diffraction pattern width were neglected. The same will be done in the calculations that follow. It is justifiable to drop terms of order 2" or less since such terms do not reveal anything of interest regarding the focusing properties of the laminae.

Let the direction cosines of the reflected ray be k, m, n. These must satisfy the following three equations.

$$k^2 + m^2 + n^2 = 1 \tag{13}$$

$$k \cos(\theta_o + \eta) + m \sin(\theta_o + \eta) = -\sin\theta \tag{14}$$

$$\begin{vmatrix} k & m & n \\ \cos(\theta_o + \eta) & \sin(\theta_o + \eta) & 0 \\ \dfrac{\sin(2\theta_o + \eta + t)}{a} & \dfrac{-\cos(2\theta_o + \eta + t)}{a} & \dfrac{b}{a} \end{vmatrix} = 0$$

where eq. (14) insures that the reflected ray makes an angle

---

* σ and π refer to the two components of polarization; the former has its electric vector in the plane of incidence and the latter at right angles to it. In the case of no absorption $F_{\substack{\sigma \\ \pi}} = I^D_{\substack{\sigma \\ \pi}}$ where $I^D_{\substack{\sigma \\ \pi}}$ are the Darwin functions for the two types of polarization, given in Compton and Allison p. 391.

$\pi/2 - \theta$ with the normal to the crystal planes, $\overline{P\beta}$, and the determinant insures that it be coplanar with $\overline{P\beta}$ and $\overline{SP}$. The determinant reduces to:

$$k \sin(\theta_o + \eta) - m \cos(\theta_o + \eta) = \frac{n}{b} \cos(\theta_o + t) \qquad (15)$$

Multiplying (14) and (15) first by $\cos(\theta_o + \eta)$ and $\sin(\theta_o + \eta)$ respectively and adding, and then by $\sin(\theta_o + \eta)$ and $-\cos(\theta_o + \eta)$ respectively and adding, one obtains

$$k = (n/b) \cos(\theta_o + t) \sin(\theta_o + \eta) - \sin\theta \cos(\theta_o + \eta) \qquad (16)$$

$$m = -(n/b) \cos(\theta_o + t) \cos(\theta_o + \eta) - \sin\theta \sin(\theta_o + \eta) \qquad (17)$$

which, when substituted in (13), gives

$$n^2 = \frac{b^2 \cos^2\theta}{b^2 + \cos^2(\theta_o + t)}$$

From (7)

$$\cos^2\theta = \frac{b^2 + \cos^2(\theta_o + t)}{a^2} \qquad (18)$$

Substituting (18) in the expression for n^2 and taking the square root, we obtain

$$n = b/a \qquad (19)$$

Finally upon substitution of (7) and (19) in (16) and (17), the direction cosines k, m, n, are reduced to their simplest form

$$\begin{aligned} k &= (1/a) \sin(\eta - t) \\ m &= -(1/a) \cos(\eta - t) \\ n &= b/a \end{aligned} \qquad (20)$$

Note that the direction cosine in the z direction for both the incident and reflected ray are the same. This is obvious if one thinks of the crystal as being a plane mirror in the z direction.

Assuming the second crystal is removed momentarily, then the projection of the ray, represented by k, m, n, on the focal plane is the line $\overline{PF}$ where F is displaced from F_o by an angle 2t, just as S is with respect to S_o. Since the position of the point F depends on the variables t and t_z only, and not on η, then all rays from S will focus in a straight vertical line passing through F. Furthermore, since no approximations were involved in deriving the expressions for k, m, n, the focusing occurs without any aberrations, however, the line through F contains all wavelengths in the neighborhood of λ_o. To see this, we must consider eq. (12a) and note that reflections occur only when $\theta - \theta_B = 0$, where the equality holds to within the diffraction pattern width. Thus, if S and hence t is fixed, then λ is a function of z, with λ decreasing with increasing $|z|$.

Since to each point S there corresponds a point F, this implies that given a sufficiently wide spectral band of wavelengths the width of the line focus could be essentially the width of the target, approximately 1 mm. However, neglecting the continuous x-ray spectrum, the range of wavelengths permitted to go through is approximately 3 times the full width at half maximum of the K_{α_1} line, so that the line focus appears to be about 1/3 mm. wide.

If instead of keeping t fixed, as was done above, λ is kept fixed, then (12a) shows the dependence of t on z. The dependence is such that "lines" of equal λ are parabolas whose

branches extend in the positive t direction, i.e. toward the longer wavelengths.

In order to be able to trace the ray any further, it is necessary to describe it in the coordinate system of the second crystal x', y', z'. The latter axes are oriented in the same manner with respect to the second crystal as x, y, z are with respect to the first.

The relation between the two coordinate systems is given by

$$\begin{aligned} x' &= \cos(\theta_o + \alpha) - z \\ y' &= 2\sin(\theta_o - \alpha) - y \\ z' &= \cos(\theta_o + \alpha) - x \end{aligned} \tag{21}$$

where $\cos(\theta_o + \alpha) = \overline{CC_p} = \overline{C'C'_p}$ and $2\sin(\theta - \alpha) = \overline{C_pC'_p}$ as seen from Fig. 5.

Let the direction cosines of the reflected ray in the primed coordinate system be k', m', n', and in view of the above transformations, and eqs. (20)

$$\begin{aligned} k' &= -n = -b/a \\ m' &= -m = \cos(\eta - t)/a \\ n' &= -k = -\sin(\eta - t)/a \end{aligned} \tag{22}$$

Let the coordinates of the point P in the primed system be x'_1, y'_1, z'_1, then

$$\begin{aligned} x'_1 &= \cos(\theta_o + \alpha) - z \\ y'_1 &= 2\sin(\theta_o - \alpha) - \sin\phi \\ z'_1 &= \cos(\theta_o + \alpha) - \cos\phi \end{aligned}$$

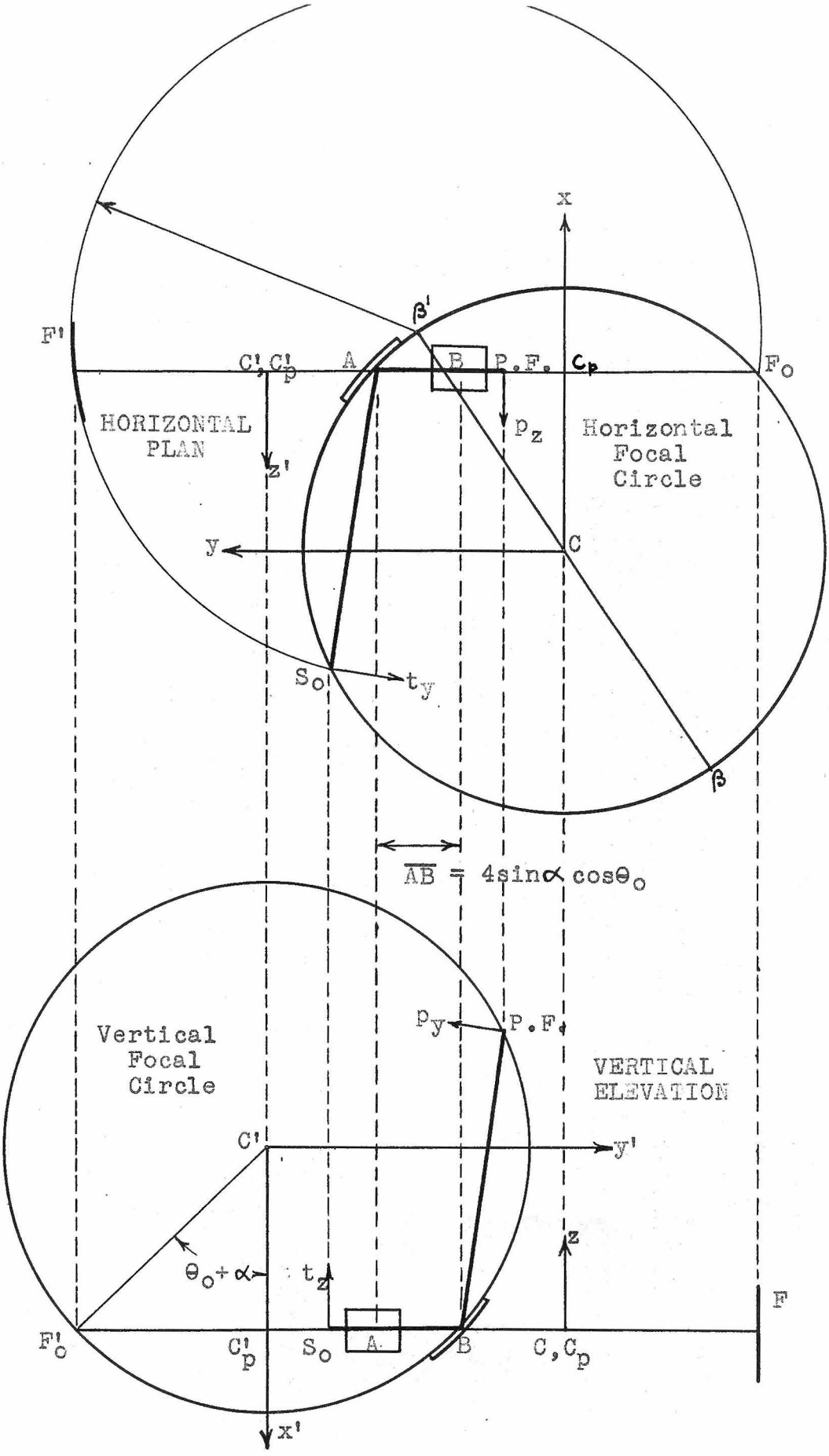

Fig. 5 - Horizontal and vertical focal circles shown together with their respective coordinate axes.

Also let the coordinates of the point P', where the ray strikes the second crystal, be x', y', z' which in terms of cylindrical coordinates are given by

$$x' = \cos\phi'$$

$$y' = \sin\phi'$$

$$z' = z'$$

so that

$$\frac{\cos\phi' - \cos(\theta_o+\alpha)+z}{n} = \frac{\sin\phi' - 2\sin(\theta_o-\alpha)+\sin\phi}{m} = \frac{z' - \cos(\theta_o+\alpha)+\cos\phi}{k}$$

or

$$\cos\phi' = \cos(\theta_o+\alpha) - z + (n/m)\left[\sin\phi' - 2\sin(\theta_o-\alpha)+\sin\phi\right] \qquad (23)$$

$$z' = \cos(\theta_o+\alpha) - \cos\phi + (k/m)\left[\sin\phi' - 2\sin(\theta_o-\alpha)+\sin\phi\right] \qquad (24)$$

It is necessary to solve eq. (23) for ϕ', or for η', where by analogy to eq. (1), we let,

$$2\eta' = \phi' - \theta_o - \alpha \qquad (25)$$

where $2\eta'$ is the central angle $\widehat{BC'P'}$, so that,

$$\cos\phi' \approx (1 - 2\eta'^2)\cos(\theta_o + \alpha) - 2\eta' \sin(\theta_o + \alpha) \qquad (26)$$

$$\sin\phi' \approx \sin(\theta_o + \alpha) + 2\eta' \cos(\theta_o + \alpha)$$

Similarly from (1)

$$\cos\phi \approx (1 - 2\eta^2)\cos(\theta_o + \alpha) - 2\eta \sin(\theta_o + \alpha)$$

$$\sin\phi \approx \sin(\theta_o + \alpha) + 2\eta \cos(\theta_o + \alpha) \qquad (27)$$

From (20)

$$\frac{n}{m} = \frac{b}{-\cos(\eta - t)} \approx -b \qquad (28)$$

where from (5)

$$b \approx \frac{z\left[1 + \eta\cot(\theta_o - \alpha)\right] - t_z}{2\sin(\theta_o - \alpha)} \qquad (29)$$

Substituting eqs. (26 to 29) in (23), and neglecting terms of order higher than z^2, η^2 or $z\eta$, as was done above, a quadratic equation in η' is obtained, which is as follows:

$$\eta'^2 \cot(\theta_o+\alpha)+\eta' = \frac{z}{2\sin(\theta_o-\alpha)}\left[1 + \frac{z\cot(\theta_o+\alpha)}{2\sin(\theta_o-\alpha)} + \eta\cot(\theta_o-\alpha) - \frac{2\eta\sin\alpha\sin\theta_o}{\sin(\theta_o+\alpha)}\right] \qquad (30)$$

$$- \frac{t_z \sin\alpha\cos\theta_o}{\sin(\theta_o-\alpha)\sin(\theta_o+\alpha)}$$

By substitution of $|z| \leq 1/60$, $|\eta| \leq 1/80$, and $\alpha \approx 1/30$ radians, it is found that the next to the last term in the preceding equation is of the order of 2" and hence may be neglected.

The quadratic equation is of the form

$$A\eta'^2 + \eta' = B$$

whose solution is

$$\eta' = \frac{-1 + (1 + 4AB)^{\frac{1}{2}}}{2A} \approx B - AB^2$$

Applying the above equation to (30) the following result is obtained,

$$\eta' = \frac{z}{2\sin(\theta_o-\alpha)}\left[1 + \eta\cot(\theta_o-\alpha)\right] - \frac{2t'\sin\alpha\cos\theta_o}{\sin(\theta_o-\alpha)} \qquad (31)$$

where

$$t' \equiv t_z/2\sin(\theta_o + \alpha)$$

and plays the same role in the primed coordinate system as t does in the unprimed system, $|t'| \leq 1/1500$ radians.

To solve for z', we substitute $k/m = -\tan(\eta - t)$ together with eqs. (26), (27) and (31) into (24), which after simplification becomes

$$z' = 2\eta \sin(\theta_o - \alpha) - \frac{z\eta \cos(\theta_o + \alpha)}{\sin(\theta_o - \alpha)} + 4t \sin\alpha \cos\theta_o \qquad (32)$$

The direction cosines of the normal to the crystal planes at P' are given by (6), with η' replacing η. They are:

$$\cos(\theta_o + \eta'), \quad \sin(\theta_o + \eta'), \quad 0 \qquad (33)$$

The direction of the ray incident on the second crystal k', m', n' are given in terms of b, η, t by eqs. (22).

Let the angle between the above two directions be $\pi/2 - \theta'$ where θ' is the grazing angle. Therefore,

$$\begin{aligned}\cos\left(\frac{\pi}{2} - \theta'\right) = \sin\theta' &= k' \cos(\theta_o + \eta') + m' \sin(\theta_o + \eta') \\ &\approx -b\cos(\theta_o + \eta') + (1 - b^2/2)\cos(\eta - t)\sin(\theta_o + \eta') \\ &\approx -\left[b + \frac{(\eta - t)^2}{2} \tan(\theta_o + \eta')\right] \cos(\theta_o + \eta') \\ &\quad + (1 - b^2/2) \sin(\theta_o + \eta') \qquad (34)\end{aligned}$$

where eqs. (5), (8) and (22) were used in the second step, and in the last step $\cos(\eta - t)$ was expanded into $1 - (\eta - t)^2/2$. Let

$$\gamma' = b + \frac{(\eta - t)^2}{2} \tan(\theta_o + \eta') \qquad (35)$$

Since γ' is a small quantity, it is permissible to rewrite eq. (34), thus:

$$\begin{aligned}\sin\theta' &\approx -\sin\gamma' \cos(\theta_o + \eta') + \cos\gamma' \sin(\theta_o + \eta') \\ &= \sin(\theta_o + \eta' - \gamma')\end{aligned}$$

from which it is easily seen that

$$\theta' = \theta_o + \eta' - \gamma'$$

With the help of (29), eq. (35) can be simplified by dropping higher order terms, namely those involving t. Thus,

$$\gamma' = \frac{z}{2\sin(\theta_o - \alpha)}\left[1 + \eta\cot(\theta_o - \alpha)\right] + \frac{\eta^2}{2}\tan\theta_o - \frac{t'\sin(\theta_o + \alpha)}{\sin(\theta_o - \alpha)}$$

combining the above with (31), results in

$$\theta' = \theta_o + t' - \frac{\eta^2}{2}\tan\theta_o \tag{36}$$

As in the case of the first reflection, we are interested in the difference between the grazing angle θ', and the Bragg angle θ_B for the wavelength λ. Making use of (11), the final result is,

$$\theta' - \theta_B = t' - \frac{\eta^2}{2}\tan\theta_o - \frac{\lambda - \lambda_o}{\lambda_o}\tan\theta_o \tag{37}$$

The above equation can now be compared with (12a), which is,

$$\theta - \theta_B = t - \frac{z^2\tan\theta_o}{8\sin^2(\theta_o - \alpha)} - \frac{\lambda - \lambda_o}{\lambda_o}\tan\theta_o \tag{38}$$

The conditions that must be imposed on $(\theta - \theta_B)$ and $(\theta' - \theta_B)$ in order that a ray of wavelength λ be reflected by both crystals are,

$$\theta - \theta_B = \theta' - \theta_B = 0 \tag{39}$$

where the equality is to be understood to hold to within the diffraction width, namely 2" of arc. This, incidentally, is another justification for dropping small order terms.

In view of the above requirements eqs. (37) and (38) show some interesting properties of the crystals. For purposes of computation it is better to rewrite the above equation in

numerical form by substituting $\theta_o = 40.7^o$ and $\alpha = 2.1^o$,

$$\theta' - \theta_B = t' - 0.430\eta^2 - 0.860(\lambda - \lambda_o)/\lambda_o \quad (40)$$

$$\theta - \theta_B = t - 0.276z^2 - 0.860(\lambda - \lambda_o)/\lambda_o \quad (41)$$

Subtracting (37) from (38), gives the dependence of η and z on t and t' alone,

$$(\eta^2/2)\tan\theta_o - z^2\tan\theta_o/8\sin^2(\theta_o - \alpha) = t' - t \quad (42)$$

or

$$0.430\eta^2 - 0.276z^2 = t' - t \quad (42a)$$

If the target of the x-ray tube is so small that t and t' can be neglected, or if $t' - t = 0$ in the above equation, then the area of the first crystal which is contributing to the point focus degenerates into two lines whose widths (≈ 0.01 mm.) correspond to the diffraction pattern widths and whose equations are

$$z = \pm 1.25\eta \quad (43)$$

along which the wavelength decreases with increasing $|z|$, as is given by eq. (41). By definition, 2η is the angle measured at the center C of the focal circle from the center of the crystal to the arbitrary point P, so that z and 2η may be considered as the coordinate axes of the crystal lamina with the origin at its center. If the above two lines are projected on a plane perpendicular to the incident (or once reflected) beam, then they become orthogonal and are inclined at 45^o with the horizontal plane. Since the reflecting portions of the crystal laminae were designed to admit a square beam, 3/4" x 3/4", it is obvious that the above lines connect the opposite corners of the laminae. When t' - t is <u>not</u> negligible, eq. (42) represents

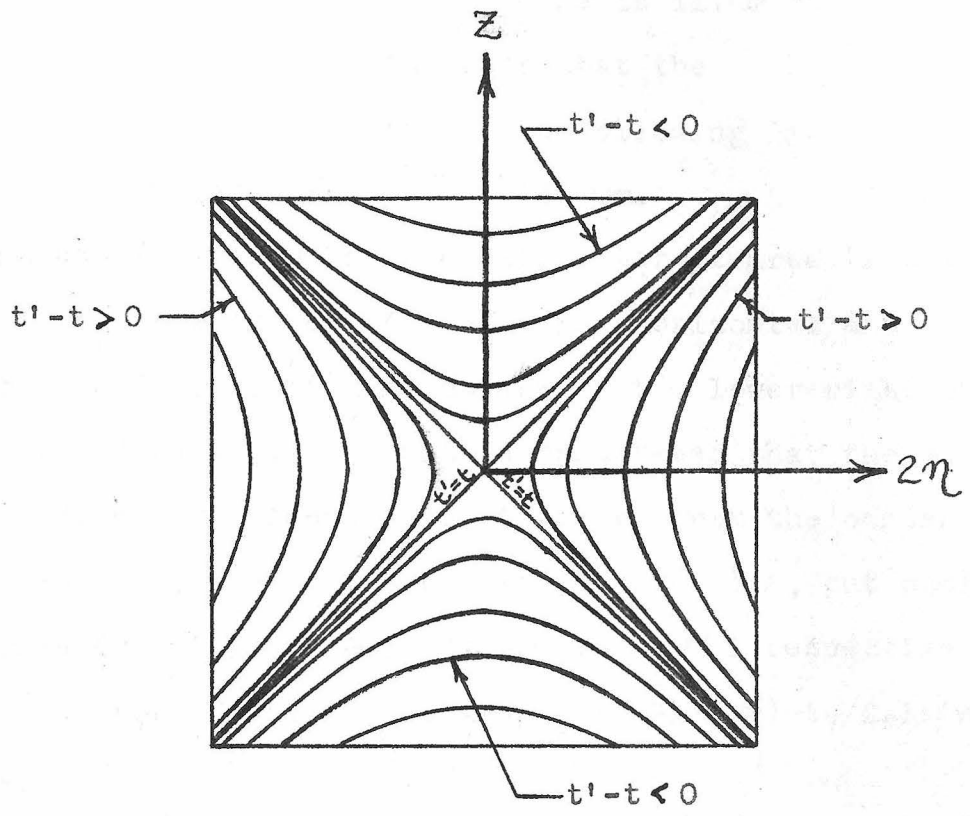

Fig. 6 - Cross-section of beam (3/4" x 3/4") midway between the two crystals. Hyperbolas represent cross-section of rays emanating from points in the target for which t'-t is a constant.

two families of hyperbolas whose asymptotes are eqs. (43). The upper and lower hyperbolas correspond to negative values of $t' - t$. When $|t' - t|$ takes on all values from zero to some finite value, eq. (42a) gives the four limiting hyperbolas within which the first crystal lamina is illuminated by x-rays. Eq. (42a) also shows that in order that the whole lamina be illuminated $t' - t$ must satisfy the following inequality,

$$-0.042 \leq t' - t \leq 0.042 \text{ mm.}$$

This inequality shows that the useful target area is a strip inclined at approximately 45° with the horizontal, and extending from the upper left hand corner to the lower right hand corner of the target. It must be remembered that the values t and t' do not represent true distances from the center of the target as seen from the center of crystal A, but must be multiplied by $2\sin(\theta_o + \alpha)$ and $2\sin(\theta_o - \alpha)$ respectively, to give t_z and t_y. Thus, $t' - t = t_z/2\sin(\theta_o + \alpha) - t_y/2\sin(\theta_o - \alpha)$ so that,

$$-0.06 \leq t_z - 1.09 t_y \leq 0.06 \text{ mm.} \qquad (43.1)$$

and the actual inclination of the strip is $47\ 1/2^{\circ}$ with the horizontal plane.

The limits on t and t' individually are given by (40) and (41) in which the maximum value of $|\lambda - \lambda_o|$ can be taken arbitrarily as 0.30 X.U., i.e. the half width at half maximum of the $K_{\alpha 1}$ line. Hence,

$$-0.10 \leq t \leq 0.14 \text{ mm.} \quad \text{or} \quad -0.13 \leq t_y \leq 0.17 \text{ mm.}$$

$$-0.10 \leq t' \leq 0.15 \text{ mm.} \quad \text{or} \quad -0.14 \leq t_z \leq 0.20 \text{ mm.}$$

It is seen that the useful target area is a diagonal strip about 0.09 mm. wide enclosed in a rectangular area 0.30 mm. x 0.34 mm., the sides of which are not symmetrically disposed about the center of the target ($t = t' = 0$), see Fig. 8a, p. 38. Note that the width of the strip is independent of the wavelength, except through the factor θ_o, as given by eq. (42).

It is known that the curves representing the intensity versus wavelength of x-ray spectral lines are "witches".* Thus, it is obvious that the area under that part of the witch (out to half-max.), which is being reflected above, is half the total area. If the full target, 1 mm. x 1 mm., is used instead, then it is not hard to show that about 83% of the area under the witch is being reflected. The useful area of the target, however, is still a diagonal strip of the same width, namely 0.09 mm. This width is independent of wavelength admitted, but depends on the size of the crystal laminae only.

Returning our attention to the ray, which was found to strike the second crystal with a grazing angle θ' at the point P' whose coordinates are $(1, \theta_o + \alpha + 2\eta', z')$, we now consider the twice reflected ray and follow it through to the point focus.

Let the direction cosines of the twice reflected ray be k", m", n", then the conditions that they must satisfy are similar to those given by (13), (14) and the determinant, with

---

*The standard equation of a "witch" at the origin is $\frac{A}{1 + x^2/w^2}$.

η' replacing η and k', m', n' replacing the last row in the determinant.

$$k''^2 + m''^2 + n''^2 = 1 \tag{44}$$

$$k'' \cos(\theta_o + \eta') + m'' \sin(\theta_o + \eta') = -\sin\theta' \tag{45}$$

$$\begin{vmatrix} k'' & m'' & n'' \\ \cos(\theta_o + \eta') & \sin(\theta_o + \eta') & 0 \\ k' & m' & n' \end{vmatrix} = 0$$

As in the case of the first reflection, the direction cosines in the z' direction of the incident and reflected rays are equal, i.e. $n'' = n'$, so that with the help of (22) we have:

$$n'' = -(1/a) \sin(\eta - t) \tag{46}$$

Subtracting the last row of the determinant from the first and expanding, we get

$$(k'' - k')\sin(\theta_o + \eta') = (m'' - m')\cos(\theta_o + \eta')$$

Eliminating $\sin\theta'$ from (45) by means of (34), we get

$$(k'' + k')\cos(\theta_o + \eta') = -(m'' + m')\sin(\theta_o + \eta')$$

Solving the last two equations for k" and m", we obtain

$$k'' = -k' \cos 2(\theta_o + \eta') - m' \sin 2(\theta_o + \eta') \tag{47}$$

$$m'' = -k' \sin 2(\theta_o + \eta') + m' \cos 2(\theta_o + \eta') \tag{48}$$

which are left in the present form for convenience.

In the ideal case the position of the point focus, relative to the primed coordinate system, must be the same as that of the center of the target relative to the unprimed system. The coordinates of the center of the target, point S_o, are $(1, 3\theta_o - \alpha, 0)$ and hence the coordinates of the point focus must be the same. The general ray that we are dealing with,

however, may not pass exactly through this point, but may pass close by, say through $(1, 3\theta_o - \alpha + 2p, p_z)$ where p and p_z are small quantities. If we let

$$p_y = 2p \sin(\theta_o - \alpha),$$

then p_y and p_z represent the coordinates of the general ray in a plane perpendicular to the central ray and passing through the point where it touches the focal circle, the coordinates of the central ray being (0, 0). See Fig. 5.

The equation of the twice reflected ray can now be written as:

$$\frac{\cos(3\theta_o - \alpha + 2p) - \cos\phi'}{k''} = \frac{\sin(3\theta_o - \alpha + 2p) - \sin\phi'}{m''} = \frac{p_z - z'}{n''} \quad (49)$$

Substituting (47) and (48) in the first two terms above, and simplifying without making any approximations, we get

$$\tan(p - \eta') = k'/m' \quad (50)$$

where use has been made of $\phi' = \theta_o + \alpha + 2\eta'$. From eqs. (22), $k'/m' = n/m = -b/\cos(\eta - t) \approx -b$, and since $\tan(p - \eta') \approx p - \eta'$, eq. (50) becomes, with the help of (31) and (29),

$$p = \eta' - b = t' \quad (51)$$

or

$$p_y = t_z \sin(\theta_o - \alpha)/\sin(\theta_o + \alpha) \quad (52)$$

To find the coordinates of the ray in the other direction, i.e. p_z, we consider again eq. (49),

$$p_z = z' + (n''/k'')\left[\cos(3\theta_o - \alpha + 2p) - \cos\phi'\right]$$

where z' is given by (32) and n"/k" is given by (46), (47) and (22). The resulting equation is,

$$p_z \approx 2t\sin(\theta_o + \alpha) = t_y \sin(\theta_o + \alpha)/\sin(\theta_o - \alpha) \quad (53)$$

Subtracting (53) from (52), we get

$$p_y \sin(\theta_o+\alpha)/\sin(\theta_o-\alpha) - p_z = t_z - t_y \sin(\theta_o+\alpha)/\sin(\theta_o-\alpha) \qquad (54)$$

or numerically

$$1.09p_y - p_z = t_z - 1.09t_y \qquad (54a)$$

which in view of the inequality (43.1) gives

$$-0.06 \leqslant p_z - 1.09p_y \leqslant 0.06 \text{ mm.} \qquad (55)$$

Eqs. (52) and (53) together with the inequalities imposed on t_z and t_y, for transmission of half the area under the $K_{\alpha 1}$ line, give

$$\begin{aligned} -0.13 \leqslant p_y \leqslant 0.18 \text{ mm.} \\ -0.14 \leqslant p_z \leqslant 0.18 \text{ mm.} \end{aligned} \qquad (56)$$

The three inequalities above show that the focal spot in the final "point" image is a strip of width 0.09 mm., inclined at 47 1/2° with the vertical focal plane. This strip is enclosed in a rectangular area 0.31 mm. x 0.32 mm. See Fig. 8a, p. 38.

We can now come to the following conclusion. The focal spot is the image of the useful portion of the target, namely, a diagonal strip 0.09 mm. wide. By varying the target aperture, it is possible to change the shape and size of the focal spot. Although the focal spot is the image of the target, the resolution of the instrument is determined by its geometry. In other words, no matter what size target is used, only a diagonal strip is useful in forming a focal spot. The length of the strip is determined by the width of the $K_{\alpha 1}$ line; beyond that only the continuous radiation is reflected. If the strip

is sufficiently long, i.e. if the target extends sufficiently along the length of the strip, about 1.8 mm., the $K\alpha_2$ line may be reflected. The latter case is shown by means of dotted lines in Fig. 8a, p. 38. This, however, is not desirable since the focal spot will then appear as two elongated dots. Any target area outside the diagonal strip is useless and only contributes to the incoherent scattering which adds to the general background in the neighborhood of the focal spot. If a tube whose target area is 1 mm. x 1 mm. is used, the focal spot is approximately 1.4 mm. x 0.09 mm.

Before concluding this section, it must be pointed out that the intensity reflected by the two crystals is a complicated expression involving the integral $F_\sigma(\theta-\theta_B)\ F_\pi(\theta'-\theta_B)$ where the arguments of the functions F are given by eqs. (40) and (41). The intensity problem will be discussed in more detail later.

ABERRATIONS

So far, only the ideal focusing system has been considered, that is, the case where the crystals have been cylindrically ground prior to bending. In practice, however, it is found to be a rather difficult task to grind crystals cylindrically with any degree of accuracy. Instead, the crystals are ground flat and then bent to twice the radius of the focal circle in order to obtain the proper curvature for the crystal planes. Thus, the concave crystal face does not everywhere hug the focal circle but is only tangent to it at the center of the crystal.

The use of initially flat crystals and their effect on the focusing qualities of single crystal monochromators has been discussed extensively by Johann[10]. Herein, we shall designate this as the approximate focusing system.

To find what happens to the focal spot when two such approximate focusing crystals are used in the point focusing arrangement, it is necessary to retrace a general ray through the system. Since it is neither instructive nor interesting to repeat the calculations in detail, only the more important results will be presented.

Fig. 7 shows a flat crystal which has been bent to a radius equal to twice the focal radius. Point P is again designated as a general point on the crystal lamina, however, it is no longer on the focal circle. C_f is the center of curvature of the crystal face and η is measured about the point C_f.

The difference between the grazing angle at the first crystal and the Bragg angle for the wavelength λ is given by

$$\theta - \theta_B = t - 0.276z^2 - 0.860(\lambda - \lambda_o)/\lambda_o + 0.628\eta^2 \qquad (57)$$

At the second crystal it is found that

$$\theta - \theta_B = t' - 0.430\eta^2 - 0.860(\lambda - \lambda_o)/\lambda_o + 0.350z^2 \qquad (58)$$

Comparing these equations with (41) and (40), it is seen that they differ only in the last term.

In order that a ray be reflected by both crystals, the two previous equations must be equated to zero as has been done before. Subtracting (57) from (58), we get an equation similar to (42),

$$1.058\eta^2 - 0.626z^2 = t' - t \qquad (59)$$

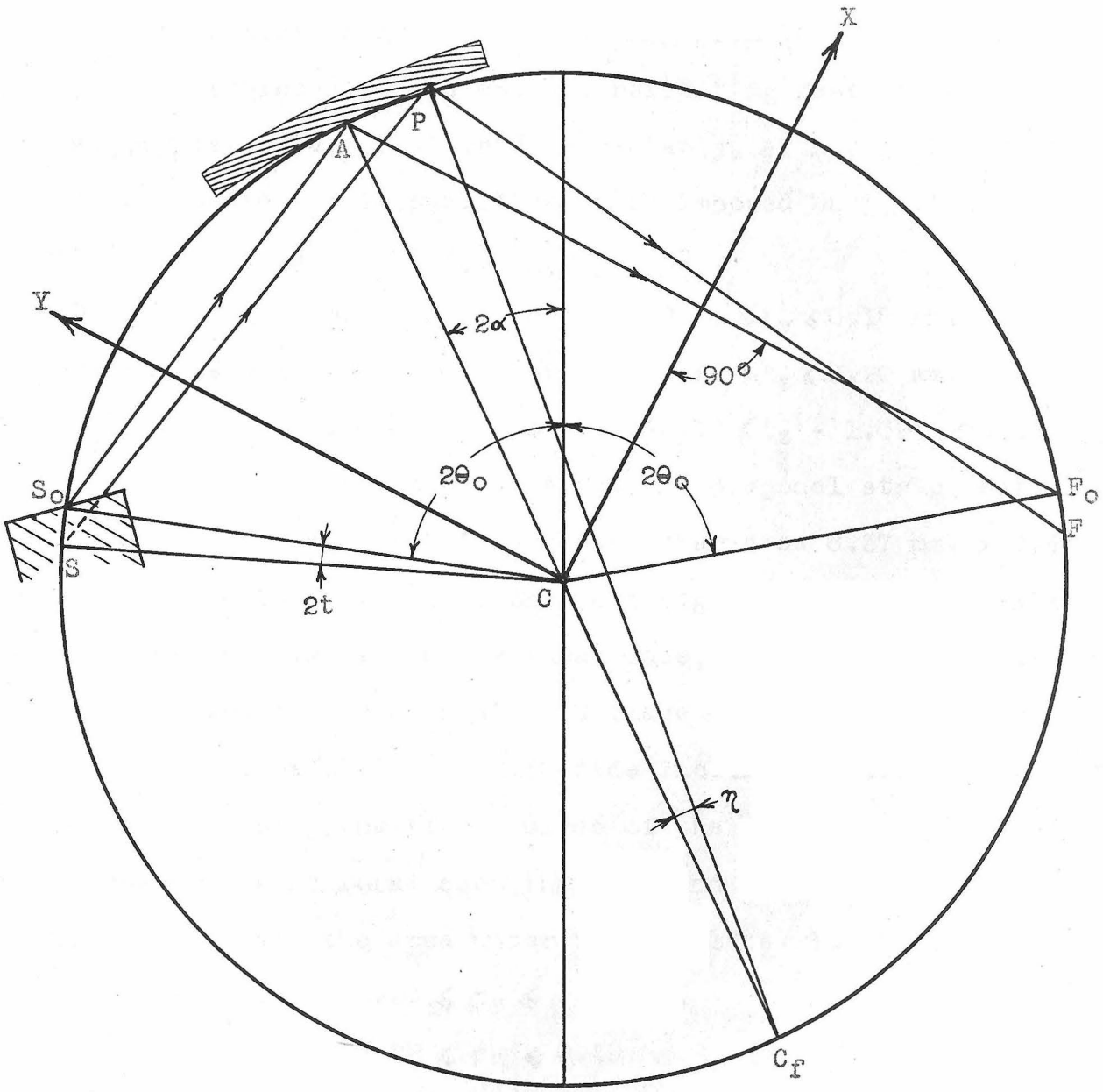

Fig. 7 - Geometry of a single bent crystal with faces flat prior to bending.

representing two families of hyperbolas whose asymptotes are

$$z = \pm 1.30\eta$$

It is thus seen that, in passing from the ideal to the approximate focusing system, the reflecting features of the two crystals are not altered appreciably, although in this latter scheme the inequalities to be imposed on t, t' and t' - t are given by (57), (58) and (59).

$$\begin{aligned} &-0.16 \leqslant t \leqslant 0.14 \text{ mm.} && \text{or} && -0.20 \leqslant t_y \leqslant 0.17 \text{ mm.} \\ &-0.16 \leqslant t' \leqslant 0.15 \text{ mm.} && \text{or} && -0.22 \leqslant t_z \leqslant 0.20 \text{ mm.} \\ &-0.10 \leqslant t' - t \leqslant 0.10 \text{ mm.} && \text{or} && -0.14 \leqslant t_z - 1.09 t_y \leqslant 0.14 \text{ mm.} \end{aligned} \qquad (60)$$

The useful target area is again a diagonal strip, but with width 0.19 mm. enclosed in a rectangular area 0.37 mm. x 0.42 mm., as is shown in Fig. 8b, p. 38. Although the length of the strip is about the same as in the ideal case, the width is doubled.

The focal spot is again the image of the useful target area, namely, a strip 0.19 mm. wide inclined at 47 1/2° with the vertical focal plane (focal plane of the second crystal). The extension of the focal spot in the y and z directions (for transmission of half the area under the K_{α_1} line) is given by,

$$\begin{aligned} -0.20 \leqslant p_y \leqslant 0.16 \text{ mm.} \\ -0.22 \leqslant p_z \leqslant 0.19 \text{ mm.} \end{aligned} \qquad (61)$$

Hence, the strip is enclosed in a rectangular area 0.36mm.x0.41mm. The whole target (1 mm x 1 mm.) will transmit about 81% of the area under the K_{α_1} line. The focal spot will then be approximately 0.19 mm. x 1.41 mm. It is interesting to note that an

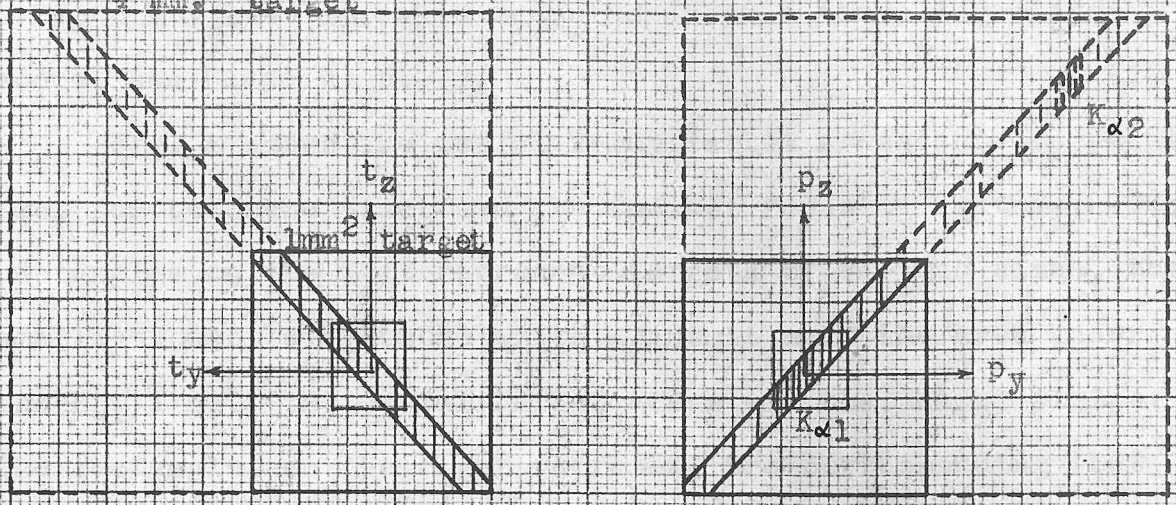

Useful target area (shaded). Focal spot (shaded).

Fig. 8a - Useful target area and focal spot in the exact focusing system.

Scale: 1 mm.

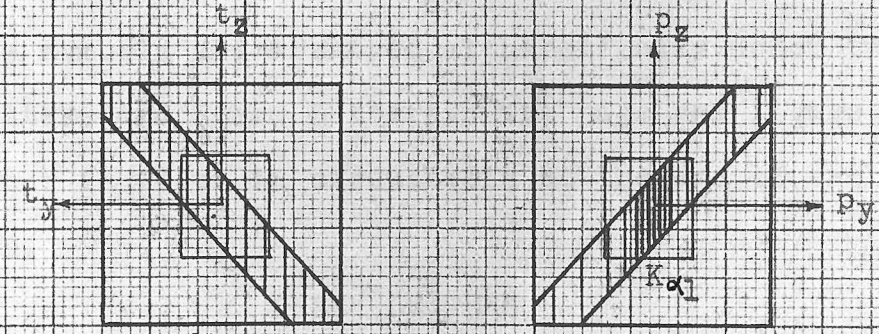

1 mm.² target Focal spot

Fig. 8b - Useful target area and focal spot in the inexact focusing system.

actual photograph of the focal spot reveals its size to be 0.196 mm. x 1.40 mm. when measured under a traveling microscope, see Plate 9, p. 70.

Fig. 8 shows the useful x-ray target areas and the point foci for both the exact and the inexact focusing systems. The rectangles on the left represent targets of various sizes, the smallest ones being those which transmit half the area under the $K_{\alpha 1}$ line. The useful target areas are the shaded strips. The rectangles on the right represent the corresponding (but not equal) areas which enclose the point foci. The latter are the shaded strips with the darker shade representing roughly the more intense portion of the foci. The directions of the coordinates t_y, t_z, p_y and p_z are shown in Fig. 5, p. 22.

This concludes the geometrical consideration of the point focusing monochromator.

TABLE OF NOMENCLATURE

The symbols are arranged alphabetically under two headings, Greek Letters and Roman Letters. The page and figure where they first occur is given in parenthesis at the end of each descriptive paragraph.

GREEK LETTERS

α The dihedral angle between the crystal plane and its face at the center of the latter (or between their normals). (P. 9 and Fig. 2)

β The generator of the focal cylinder about which the crystal planes are concentric. (P. 6 and Fig. 2).

β' The point in the focal plane diametrically opposite from β . (P. 8 and Fig. 2).

γ The small angle, referred to the horizontal focal plane, by which the grazing angle of incidence (θ) differs from the Bragg angle (θ_o), due to the vertical divergence of the incident ray. (The vertical divergence angle is the angle between the incident ray and the focal plane.) (P. 16).

γ' Small angle referred to the vertical focal plane and defined by Eq. (35). (P. 25).

η Half the central angle measured about the center of the horizontal focal circle (C), and in its plane, from the center of the first crystal (A) to the arbitrary point P. (P. 14 and Fig. 4). (Note: See also Fig. 7 for definition of η in the inexact focusing system.)

η' Same as η but referred to the vertical focal circle, the center of the second crystal (B) and the point P'. (P. 23).

θ The grazing angle or the angle between the ray and the crystal planes of the first crystal at the arbitrary point P. (pp. 8, 15 and Fig. 2).

θ' The grazing angle or the angle between the (once reflected) ray and the crystal planes of the second crystal at the point P'. (P. 23).

θ_o The Bragg angle for the wavelength λ_o at the center of the $K_{\alpha 1}$ line. (P. 12 and Fig. 4).

θ_B The Bragg angle for any wavelength λ in the neighborhood of λ_o. (P. 15).

λ_o Wavelength at the center of the $K_{\alpha 1}$ line. (P. 11).

λ Wavelength at points other than the center of the $K_{\alpha 1}$ line. (P. 17).

ϕ One of three cylindrical coordinates of the point P, the three being l, ϕ and z, with the latter perpendicular to the horizontal focal circle. (P. 11 and Fig. 4).

ϕ' Same as ϕ but for point P' and the vertical focal circle. (P. 23).

ROMAN LETTERS

A Geometrical center of 1st crystal (or crystal with horizontal focal circle.) (P. 8 and Fig. 2).

a_o Abbreviation for expression on p. 14.

a Abbreviation for expression on p. 15.

B Geometrical center of 2nd crystal (or crystal with vertical focal circle). (P. 10 and Fig. 3).

b_o Abbreviation for expression on p. 14.

b Abbreviation for expression on p. 15.

C Center of horizontal focal circle (p. 6 and Fig. 2).

C' Center of vertical focal circle (p. 11 and Fig. 3).

C_p (P. 21 and Fig. 5.)

C'_p (P. 21 and Fig. 5.)

C_f Center of curvature of crystal planes in the inexact focusing system (p. 35 and Fig. 7).

d Grating spacing of the crystal laminae used in reflection of Cu $K_{\alpha 1}$ line (p. 8).

F Point on vertical line focus at which the reflected ray from the arbitrary point P on the first crystal intersects the focal cylinder, in the absence of the second crystal. (P. 20 and Fig. 4.) (Also, in the qualitative discussion, the line focus of a single crystal, or its midpoint (p. 6 and Figs. 2, 3)).

F_o Center of vertical line focus; also called the "focal point" of the horizontal focal circle. (P. 12 and Fig. 4).

F'	Point on virtual line source (in horizontal plane) from which the arbitrary ray appears to emanate after it is reflected from the 1st crystal. (Fig. 5). (Also, in the qualitative discussion, the virtual line source or its midpoint. (p. 9 and Fig. 3)).
F'_o	Center of virtual line source (Fig. 5).
k, m, n	Direction cosines of the once reflected ray from the point P on the 1st crystal to the point P' on the 2nd crystal in the coordinate system of the former. (P. 16).
k', m', n'	Same as above but in the coordinate system of the 2nd crystal. (P. 19).
k'', m'', n''	Direction cosines of the twice reflected ray from the point P' on the 2nd crystal to the Point Focus. (P. 28).
P.F.	Point Focus. (P. 10 and Fig. 3).
P	Arbitrary point on 1st crystal at which a ray from point S is reflected. (P. 6 and Fig. 2).
P'	Point on second crystal where the once reflected ray (from point P) is again reflected. (P. 23).
p	Small angular displacement measured about the center of the vertical focal circle and in the plane of the latter where the twice reflected ray pierces the focal plane. The focal plane is the plane through the point P.F. and perpendicular to the central ray. (P. 29).
p_y, p_z	Coordinates in the focal plane* of the point where the ray pierces the latter, see above. p_z is in a direction perpendicular to the vertical focal circle and p_y is at right angles to it. (P 32 and Fig. 5).
r	Radius of either focal circle. (P. 11).
S_o	Point on horizontal focal circle representing center of x-ray target. (P. 12 and Fig. 4).
S	Point at which the arbitrary incident ray intersects the focal cylinder in the neighborhood of S_o. (P. 15 and Fig. 4).

*Plane passing through the point focus at right angles to the central ray.

t	Small angular displacement measured about the center of the horizontal focal circle and in the plane of the latter, where the arbitrary ray emerges from the target. (P. 15, and Fig. 4).
t_y, t_z	Coordinates in a plane at right angles to the central ray through the point S_o of the arbitrary ray emerging from the target. (P. 15 and Fig. 5).
(x,y,z)	Coordinate system of horizontal focal circle. (P. 11 and Figs. 4, 5).
(x',y',z')	Coordinate system of the vertical focal circle. (P. 21 and Fig. 5).
x_1', y_1', z_1'	Coordinates of point P in the primed coordinate system. (P. 21).

PART III

THE INTENSITY PROBLEM AND SUGGESTED IMPROVEMENTS

The problem of obtaining sufficient intensity is one of the most difficult in connection with the point focusing monochromator and one that has been the cause of a good deal of concern. Losses due to polarization at each reflection are inherent in the design of the instrument and can only be reduced by a decrease in the Bragg angle. (See eq. 64 below.) The latter can be accomplished by one of two means, increasing the grating spacing or decreasing the wavelength, neither of which lends itself to a wide variety of choice.

Assuming the first crystal is illuminated uniformly with x-rays, then the intensity at the point focus is given by,

$$I = (1/2)I_o C \int_{-\lambda_{max}}^{\lambda_{max}} \int_{-\theta_{max}}^{\theta_{max}} \int_{-\theta'_{max}}^{\theta'_{max}} J(\lambda - \lambda_o)\left[F_\sigma(\theta - \theta_B)F_\pi(\theta' - \theta_B) + F_\pi(\theta - \theta_B)F_\sigma(\theta' - \theta_B)\right] d\lambda\, d\theta d\theta' \qquad (62)$$

where it must be remembered that $(\theta - \theta_B)$ and $(\theta' - \theta_B)$ are given by eqs. (41) and (40) respectively.

C is a factor depending on the thickness of the crystal, its diffraction pattern width, radius of curvature, average extinction coefficient and linear absorption coefficient. According to the dynamical theory of x-ray reflection from crystals, the condition for one hundred percent reflection (in the absence of absorption) occurs when $\theta - \theta_B$ and $\theta' - \theta_B$ are less than half the diffraction width. Outside that range

very little reflection occurs. This will be obvious as soon as the functions F_σ and F_π are written down explicitly. When the condition for complete reflection is satisfied at the surface, the incident rays are said to be rapidly "extinguished". In other words, they are reflected before they have a chance to penetrate very far into the crystal. However, when the condition is not satisfied at the surface as is the case with a target of finite size, the rays penetrate into the crystal, suffering attenuation due to absorption until they reach crystal planes for which the condition is satisfied, in which case, they are then rapidly extinguished. This situation is only possible with curved crystals in which the grazing angle changes as the beam penetrates the lattice. The reflecting properties of bent crystals have been the subject of a recent doctoral thesis and have been reported in J. App. Phys.(11)

$J(\lambda - \lambda_0)$ is the spectral distribution function. The functions F_σ and F_π , according to the theory of Darwin and for the case of negligible absorption, are given by,

$$= \left[\frac{F/Z}{\ell - \sqrt{\ell^2 - F2/Z2}}\right]^2 \qquad \text{when } \ell < -F/Z$$

$$F_\sigma(\ell) = 1 \qquad \text{when } -F/Z < \ell < F/Z$$

$$= \left[\frac{F/Z}{\ell + \sqrt{\ell^2 - F2/Z2}}\right]^2 \qquad \text{when } \ell > F/Z$$

$$= \left[\frac{F/Z}{\ell - \sqrt{\ell^2 - F^2/Z^2 \cos^2 2\theta_o}} \right]^2 \quad \text{when } \ell < -(F/Z)\cos 2\theta_o$$

$$F_\pi(\ell) = 1 \quad \text{when } -(F/Z)\cos 2\theta_o < \ell < (F/Z)\cos 2\theta_o$$

$$= \left[\frac{F/Z}{\ell + \sqrt{\ell^2 - (F^2/Z^2)\cos^2 2\theta_o}} \right]^2 \quad \text{when } \ell > (F/Z)\cos 2\theta_o$$

where $\ell = (\theta - \theta_B)\sin 2\theta_o / 2\delta - 1$

F is the crystal structure factor

Z is the total number of electrons per unit cell

δ = 1 - index of refraction

σ and π are defined in footnote page 18.

It has been shown in Compton and Allison[8] p. 397 that

$$\int_{-\infty}^{\infty} F_\sigma(\ell)\, d\ell = \frac{8F\delta}{3Z\sin 2\theta_o}$$

$$\text{and} \quad \int_{-\infty}^{\infty} F_\pi(\ell)\, d\ell = \frac{8F\delta\cos 2\theta_o}{3Z\sin 2\theta_o} \qquad (63)$$

However, in eq. (62) the arguments of F_σ and F_π are not independent but are related through eqs. (41) and (40), so that the above integrals do not apply. Attempts to integrate (62) analytically have failed.

To have some idea as to the intensity reflected by the two crystals, let us assume that C = 1, $\lambda = \lambda_o$, $z = \eta = 0$, that is, we shall consider surface reflections <u>from the centers</u> of the two crystals for one wavelength only. Eqs. (41) and (40) then become,

$$\theta - \theta_B = t$$

$$\theta' - \theta_B = t'$$

where t and t' are independent variables ranging from +1/1500 rad. to -1/1500 rad. or 144" to -144". Since the functions F_σ and F_π fall quite rapidly outside the range of complete reflection, it is justifable to set the ranges of integration on t and t' from ∞ to $-\infty$.

Setting $J(\lambda - \lambda_o) = 1$, we have, therefore,

$$I = (1/2)I_o \int_{-\infty}^{\infty}\int_{-\infty}^{\infty}\left[F_\sigma(t)F_\pi(t') + F_\pi(t)F_\sigma(t')\right]dtdt'$$

and in view of eqs. (63)

$$I = I_o\left[\frac{8F\delta}{3Z\sin 2\theta_o}\right]^2 \cos 2\theta_o \qquad (64)$$

The loss in intensity due to polarization manifests itself in the term $\cos 2\theta_o$ which is due to the function F_π . Eq. (64), though not applicable to the crystals as a whole, nevertheless gives a fair indication as to the reflection ability in the neighborhood of their centers. This equation can be used as a criterion for comparison with other crystals, and suggest the use of a crystal for which the values of F/Z, δ and $\cos 2\theta_o$ are larger than the corresponding values in quartz. Although there are numerous crystals that satisfy the above conditions, there are very few that are sufficiently large in size and have the necessary elastic properties for bending. A search of the literature has revealed only one crystal that is comparable to quartz in strength, namely topaz. It will be of interest to compare the properties of quartz and topaz.

	Quartz	Topaz	
Formula	SiO_2	$[Al(F,OH)]_2SiO_4$	
Planes used	(310)	(303)	(006)
Grating spacing, d	1.178Å	1.352Å	1.395
Molecules/unit cell	3	4	4
Electrons/unit cell, Z	90	360	360
Volume of unit cell, V	112Å^3	341.5Å^3	341.5Å^3
Crystal structure factor, F	21.8	139.0	124.4

From Compton and Allison[8] p. 280

$$\delta = \frac{(Z/V)e^2 \lambda_o^2}{2\pi mc^2} \qquad (65)$$

where e^2/mc^2 is the classical radius of the electron (2.817×10^{-5}Å), and $\lambda_o = 1.537$Å.

The Bragg angle is given by

$$\theta_o = \sin^{-1}(\lambda_o/2d) \qquad (66)$$

We can now substitute numbers into (66), (65) and (64) and get

	Quartz	Topaz	
Planes	(310)	(303)	(006)
θ_o =	40.7°	34.6°	33.4°
cos $2\theta_o$ =	0.1497	0.3555	0.3940
δ =	0.85×10^{-5}	1.12×10^{-5}	1.12×10^{-5}
F/Z =	0.242	0.386	0.346
I/I_o	4.6×10^{-12}	54×10^{-12}	50×10^{-12}

One can, therefore, expect an increase in beam intensity (at the surface) by replacing the quartz crystals with topaz

of about 54/4.6 = 12 times or 50/4.6 = 11 times depending on the planes used.

Since it is possible to obtain reflections from planes within the crystals as well, it is necessary to take into account the function C. We shall still restrict ourselves to the centers of the crystals. The function C is given by $C = C_\sigma C_\pi$ where [11]

$$C_{\sigma\atop\pi} = \left\{1-\exp\left[-\mu T(\sin(\theta_o+\alpha)+\sin(\theta_o-\alpha))/\sin(\theta_o+\alpha)\sin(\theta_o-\alpha)\right]\right\}\cdot$$
$$\left\{1-\exp\left[-\epsilon_{ave} w_{\sigma\atop\pi} R/\cos\theta_o\cos\alpha(1+\sin^2\alpha)\right]\right\} \div \qquad (67)$$
$$\left\{1-\exp\left[-\mu w_{\sigma\atop\pi} R(\sin(\theta_o+\alpha)+\sin(\theta_o-\alpha))/\sin(\theta_o-\alpha)\cos\theta_o\cos\alpha(1+\sin^2\alpha)\right]\right\}$$

where μ = linear absorption coefficient

T = thickness of the crystals = 0.07 cm.

R = radius of curvature = 120 cm.

ϵ_{ave} = average extinction coefficient

α = angle between crystal planes and faces

$w_{\sigma\atop\pi}$ = diffraction pattern widths

Although eq. (67) is supposed to express the area under a rocking curve it is applicable here. In the case of a rocking curve experiment, a fine parallel beam of x-rays strikes a crystal which is rotated a few seconds of arc at a time, the reflected beam being measured in each position. In our case, because of the finite size of the target, rays from different parts of it converge and strike the center of the crystal with different grazing angles so that the total intensity is equal to the area under the rocking curve mentioned in the previous case.

We again compare quartz and topaz. However, it is first necessary to compute μ, ϵ_{ave} and w_{σ} , w_{π} .

$$\mu = g\sum_i p_i \mu_i$$

where g = density of crystal

p_i = mass of element i in the crystal / total mass

μ_i = mass absorption coefficient of element i

$$\epsilon_{ave} = \frac{3\pi e^2 \lambda_o F}{8\, mc^2 V} = 5.09 \times 10^3 (F/V) \text{ cm}^{-1}$$

$$w_{\sigma} = (4/3) 4\delta (F/Z) \csc 2\theta_o$$

$$w_{\pi} = (4/3) 4\delta (F/Z) \cot 2\theta_o$$

where the factor 4/3 is applied to the actual width in order to approximate the actual diffraction pattern by a rectangular pattern of the same area. This approximation has been used in deriving eq. (67).

The composition and specific gravity of the two kinds of crystals are given in the following table:

		Quartz	Topaz	Mass absorption coefficient μ_i
Composition,	p_i	Si 41.7% O 53.3%	Si 15.17% O 34.67% Al 29.58% F 20.58%	Si 60.0 O 11.16 Al 49.0 F 17.0
Specific gravity		g = 2.65	3.53	

from which the values of μ can be calculated.

	Quartz	Topaz	
planes	(310)	(303)	(006)
Linear absorption coefficient	μ = 82cm^{-1}	109cm^{-1}	109cm^{-1}
Average extinction coefficient	ϵ_{ave} = 990 cm^{-1}	2070cm^{-1}	1850cm^{-1}
Diffraction pattern widths	w_{σ} = 1.112x10^{-5} w_{π} = 0.166x10^{-5}	2.462x10^{-5} 0.875x10^{-5}	2.254x10^{-5} 0.886x10^{-5}

Substituting the above values into eq. (67) together with T = 0.07 cm. and $\alpha = 2.1^{\circ}$, it is seen that the argument of the first exponential term is very large, so that the first bracketed term is equal to unity. This indicates that our crystals are sufficiently thick and that the function C does not depend on their thickness.

Hence, for the two kinds of crystals and two types of polarization, we have

	Quartz	Topaz		Ratio, Topaz to Quartz	
		(303)	(006)	(303)	(006)
σ polarization	$C_{\sigma} = 3.12$	1.78	1.90	0.57	0.61
π polarization	$C_{\pi} = 5.19$	3.65	3.61	0.70	0.70

The above calculations are based on reflections from a single bent crystal. When applied to the two crystal monochromator, the above ratios must be multiplied by one another since the σ polarization for one crystal is the π polarization for the other and vice versa. Although these ratios are unfavorable, the factors of 12 and 11 obtained previously, more than compensate for them. When the latter are taken into account, the gain in intensity with topaz is

4.8 for the (303) planes.

4.7 for the (006) planes.

It must be remembered that the above calculations were carried out for the centers of the crystals only and may not be valid for the whole crystals. However, on the basis of experimental work conducted by Ingelstam[12], the actual gain in intensity

from bent topaz crystals is not far different from the above figures.

Other means of increasing the intensity consist in enclosing the beam in helium, and using a beam which emerges with a smaller grazing angle from the target. Since the total path length of the beam is about 150 cm., the loss due to absorption in air is considerable. The substitution of helium for air improves the intensity by a factor of 3.5. The beam intensity at a smaller angle of emergence is about 2.5 times as great per unit target area. However, the projected target area is reduced by about a factor of five. Since the useful target area is a strip no larger than 0.2 mm. wide, the use of such a beam is justifiable. Taking the above factors (substitution of topaz for quartz, use of helium atmosphere, and reorientation of x-ray tube) into consideration, one can, therefore, expect a gain of 42 in intensity in the case of the (303) planes of topaz or of 41 in the case of (006) planes over the intensity available before making these changes.

PART IV

DESCRIPTION OF THE POINT FOCUSING MONOCHROMATOR

The problem of orienting two bent crystals correctly in space involves twelve independent degrees of freedom. It is not hard to see then, that unless some method is devised for lining up the crystals, in a logical or systematic manner, the solution to the problem by cut-and-try adjustment is next to impossible. The instrument which we shall describe below was designed and built with this problem in mind.

The instrument is built mainly out of steel. To avoid as much as possible any unpredictable lining up problems, all defining surfaces are surface ground with the exception of the pads on the triangular table. The cylindrical faces of the crystal clamping blocks (approximately 120 cm. in radius) are both ground and lapped by a special method described by DuMond, Lind and Cohen[13]. This shop method has the advantages that it automatically insures: (1) that the generators of the precision cylindrical clamping surfaces shall be truly normal to plane ground reference faces on the top and bottom of the crystal clamping blocks and, (2) that the radii of curvature on blocks for crystals A and B shall be closely equal. All welded parts were heat treated to prevent distortion in time.

Because of its three dimensional character, the instrument and its lining up procedure are best described by a series of plates.

PLATE 1

This is an overall view of the instrument with the parts assembled for use except that the crystals and the front halves of the crystal clamping blocks have been removed. It consists of a triangular steel table mounted by means of leveling screws on three concrete pillars. The table is provided with a number of pads which are welded to it and which are machined accurately so as to define a common reference surface. The crystal laminae are cylindrically bent by clamping between pairs of steel crystal bending blocks of which only the rear members are shown in the photograph. The block with vertical generators (crystal A) is mounted on a horizontal radius arm (R), while the block with horizontal generators (crystal B) is mounted on a radius arm (R') in the vertical plane. The area of the rectangular hole in the block marked (A) is approximately the effective crystal area. (See Plate 6 for a close-up view of the crystal blocks with crystals clamped between front and back members.) The vertical structure in Plate 1 supports the detecting device at the top (P) and the scattering sample at the bottom (S). The detecting device at present is a film holder, but provision is made for a Geiger counter which will be used when a beam of sufficient intensity is attained.

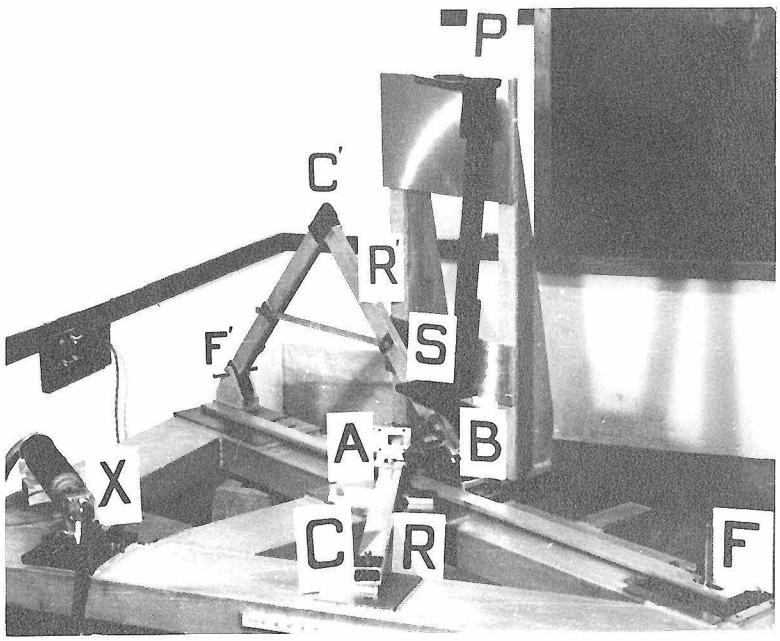

PLATE 1 - This is an overall view of the instrument with the x-ray tube X on the left, crystal blocks (rear halves) A and B at the center, and the point focus P at the top.

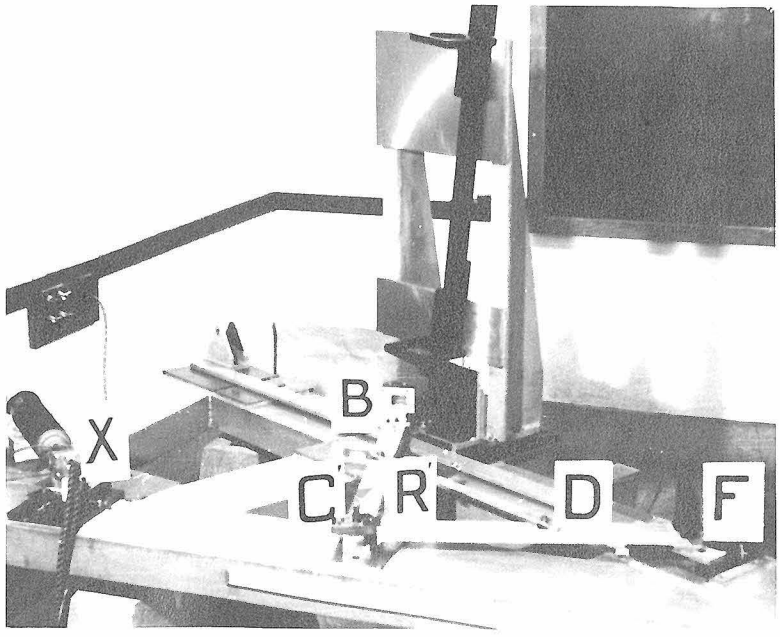

PLATE 2 - For the purpose of alignment, crystal B, with its associated radius arms R' and D, is mounted in the horizontal position as shown, R' and D, being free to turn independently about C'.

The beam diverges from the x-ray tube (X) and proceeds to crystal A, where it is Bragg-reflected ($CuK\alpha_1$), so that in the absence of crystal B, it would come to a vertical line focus at F. However, crystal B intercepts the beam and by Bragg reflection, in the vertical plane, brings the twice reflected beam to a point focus at P. We shall refer to the centers of the reflecting surfaces of crystals A and B simply as the points A and B.

The points X, A, and F lie on the horizontal focal circle (of crystal A), whose center is at C. The points F', B and P lie on the vertical focal circle (of crystal B), whose center is at C'. The two focal circles are congruent, with point F' corresponding to F, B to A, and P to X.

The long bar FF' pivots about a vertical axis at F, carrying with it the vertical structure and the assembly supporting crystal B. Hence the horizontal and vertical focal circles can be adjusted in such a way as to maintain the points F', A, B, and F in a straight line which is also the line of intersection of the two focal planes.

The vertical pin at F supports a film holder which allows first crystal B and then crystal A to be individually aligned photographically, while in the horizontal position. This alignment process is made clearer in the following plate.

PLATE 2

For the purpose of alignment, crystal B, with its associated radius arms R' and D, is mounted in the horizontal position

as shown, R' and D being free to turn independently about C'. The top of the crystal block is made parallel to the reference surface by means of a 1/10,000 inch dial indicator. This adjustment takes care of two rotational degrees of freedom of crystal B.

Next, a narrow line source of light, with a microscope focused to a point right above it is placed in line with C' and B. Crystal B is pivoted about a vertical axis, passing through B, until a line image due to the reflected light from the crystal face, appears right above the light source and hence in the field of view of the microscope. The light source and microscope are then moved along the line C'B until the image appears to be the sharpest. By measuring the distance between the light source and the center of crystal B, the diameter of the focal circle is determined. This permits us to set crystal B at the right distance from C', namely, half the focal diameter. This concludes the two optical adjustments which take care of one more rotational degree of freedom, making a total of three. The preceding statement may seem to be slightly contradictory, but it will be shown to be true by the concluding statement of the next paragraph.

The arm R' is then pivoted about C' until the line focus, due to Bragg reflection of the CuK_{α_1} line, appears on the film, in the cassette at F. The axis of the pin at F is then moved laterally to coincide with the line focus. Since one

end of the radius arm D is constrained to move with F, the angle between D and R' has thus been established, and the two arms are now rigidly clamped together by means of a cross-bar. This assembly is then removed and placed aside to permit alignment of crystal A, shown on the next plate. After crystal A is permanently adjusted in place, there will remain only the three translatory degrees of freedom of crystal B relative to A, which for convenience will be broken down into two rotations and one translation.

PLATE 3

In this photograph, crystal A and its radius arm are shown in their normal positions. The dial indicator and optical instruments are again used to orient the crystal correctly on its radius arm. If crystal A is identical to B, then the point F should remain fixed in position and the only adjustment is the location of point A relative to F*. This is done photographically by moving radius arm R about C, until the line focus appears at F. The arm is then clamped permanently in place and the assembly supporting crystal B is then mounted as shown in the next plate. As was mentioned before, the correct placement of crystal A eliminates six more degrees of freedom, thus making a total of nine eliminated so far.

---

*It was found, however, that the radii R and R' differed by about 6 mm., hence requiring a corresponding change in the length CF. It is hard to say how this slight difference in radii actually affects the point focus.

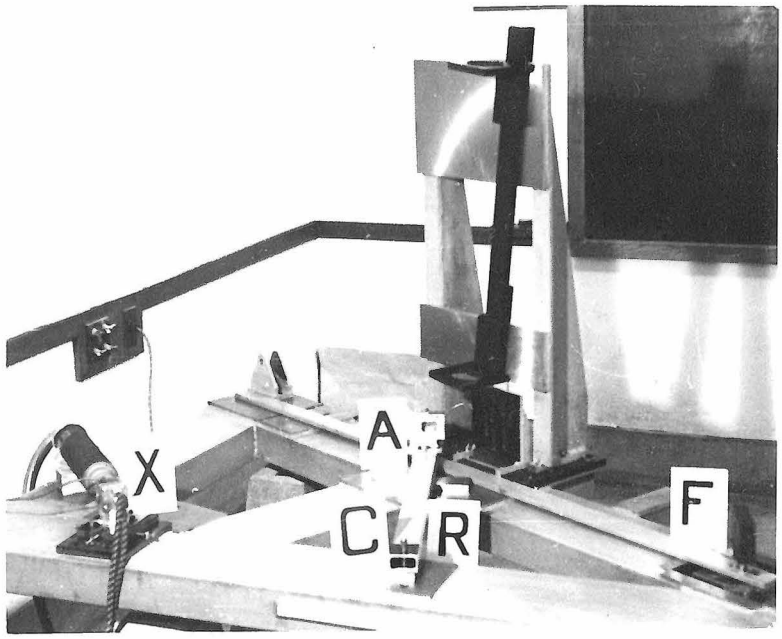

PLATE 3 - Crystal A and its radius arm R are lined up in their normal positions as shown.

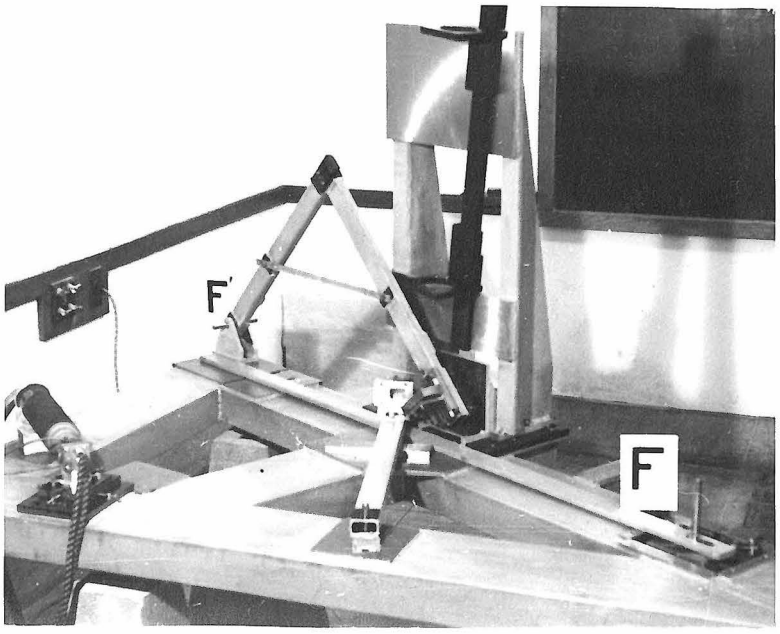

PLATE 4 - The last adjustments consist of lining up points F and F' with the center of crystal A, correcting for astigmatism and ascertaining that crystal B is set at the Bragg angle to accept radiation from A.

PLATE 4

The only adjustments left now are: (1) to line up the points F and F' with A, (2) to correct for astigmatism and, (3) to ascertain that crystal B is set at the Bragg angle to accept radiation from A. The latter adjustment is made by pivoting crystal B with its assembly about the horizontal rod at F'. The first adjustment is made by connecting two points directly above F and F' with a tight-line and pivoting the long bar FF' about the vertical rod at F until the tight-line is right above the point A. The actual point A is inaccessible, so that a scratch mark on the crystal block directly above it is used instead. Astigmatism is corrected by moving the bar FF' logitudinally, thus pulling crystal B toward or away from crystal A until the point P appears sharply defined. This adjustment is not particularly sensitive. Moving the rod one centimeter one way or another doesn't seem to make much difference.

The three adjustments, just described, eliminate the last three degrees of freedom thus concluding our lining up procedure.

PLATE 5

This plate shows the complete instrument with the exception of the lead partitions, one in front of crystal A and one between the two crystals as well as the lead box which surrounds both crystals. The partitions, consisting of a lead sheet with 3/4" x 3/4" square windows to let the beam through,

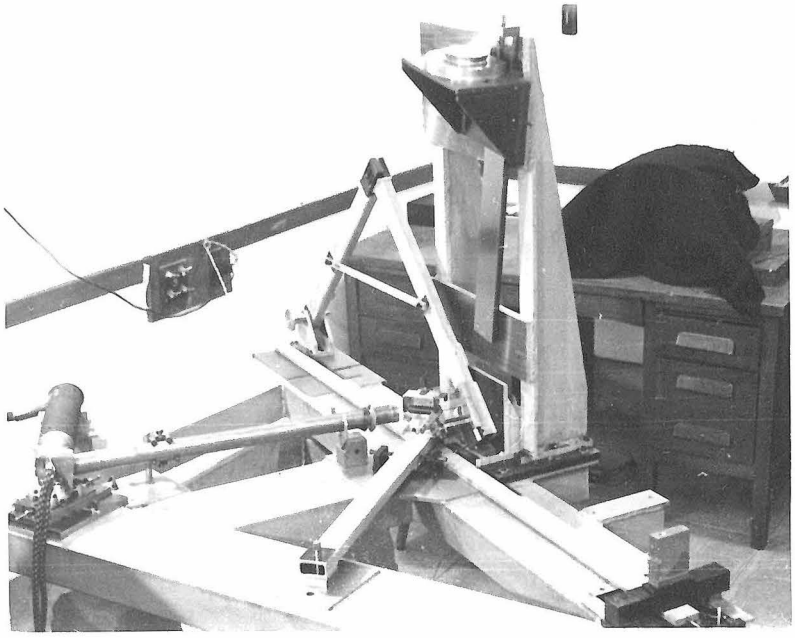

PLATE 5 - The complete instrument with the exception of the lead housing surrounding the two crystal blocks.

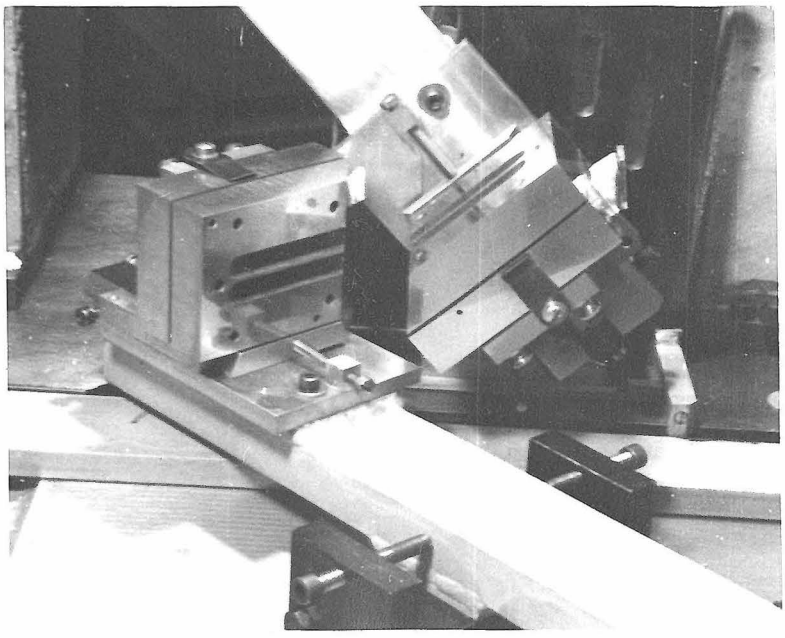

PLATE 6 - Close-up view of the crystal blocks shown with the various adjusting screws.

are used to cut down the incoherent scattering as well as fluorescent radiation from the steel crystal blocks, thus reducing considerably the background in the neighborhood of the point focus. To prevent scattering from the steel webs of the crystal blocks, the latter are covered with thin lead foil. The lead box protects the occupants of the room from irradiation. The x-ray tube is a diffraction type tube made by the Machlett Company and is driven by a North American Philips basic diffraction unit which can deliver continuously 60 PKV at a full wave rectified current rating of 50 ma. The optimum operation of the tube, however, is at 35 PKV and 20 ma. The tube that extends from the x-ray tube to crystal A is filled with helium, thus cutting down loss of intensity due to air scattering. At the top of the vertical structure one can observe the film holder mounted on an angle plate which can ride up and down on ways along the beam,thus permitting adjustment of the x-ray film to coincide with the best point focus. The scattering sample is mounted on a holder,not here shown, which can also ride up and down along the beam. Every ray which passes through the sample will be partly scattered into a narrow cone of diffusion around said ray. The resulting diffraction pattern in the focal plane is the superposition of all such scattered rays; the undeviated rays which come to a point focus being suppressed by means of a thin tungsten wire (0.020" in diam.) placed against the photographic plate. With this arrangement, every point on a circle of specified radius

concentric with the central focal spot in the focal plane receives radiation which has been scattered by every portion of the scatterer under approximately the same angle. Thus, aside from a small cosine correction coming from the fact that the rays are not parallel, the diffraction pattern represents truly the scattering property of the sample.*

THE CRYSTALS AND CRYSTAL BLOCKS

PLATE 6

This is a close-up view of the crystal blocks A and B. One can observe some of the local adjustments necessary to set crystals A and B correctly on their respective radius arms R and R'.

The blocks are made of a special type of stainless steel which is quite stable and does not distort with time. This is quite important since the curved surfaces must retain their optical properties with high precision. In order to insure uniformity of curvature, the two convex blocks were mounted on a steel plate and treated as a single unit, that is, they were cylindrically ground and lapped simultaneously. The same was done with the concave blocks. The method of grinding referred to on page 53 is shown in Plates 7 and 8.

PLATES 7 AND 8

The convex face (on the front half of the crystal block)

---

*This statement is ideally true. However, since the point focus has a finite size, a small correction must be made in regions very close to the center of the diffraction pattern.

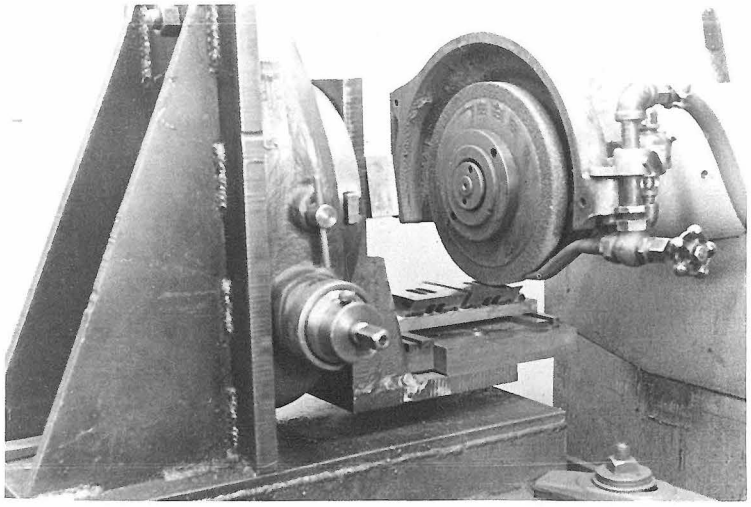

Method of generating the precision cylindrical surfaces of the curved crystal clamping blocks for the point-focusing x-ray monochromator in an ordinary flat surface grinder. The two stainless steel blocks are seen mounted on the rocking bracket under the grinder wheel. The bracket, mounted on a pivot, rocks to and fro as the work travels backward and forward on the transverse ways of the grinder. The rocking is caused by a lever arm rigidly clamped to the bracket whose far end is provided with a roller which rolls along an inclined straight-edge in unison with the transverse carriage movement.

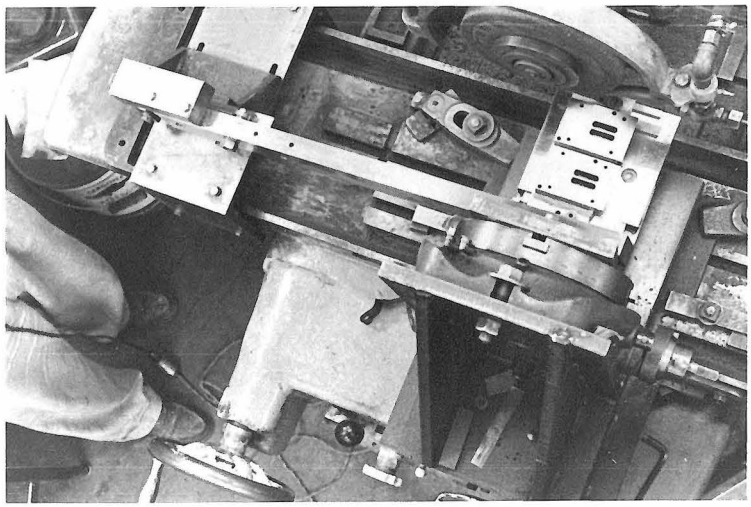

View (from above) of the method of precision profiling the cylindrical surfaces of the above mentioned clamping blocks in a flat surface grinder. The blocks can be seen mounted on the rocking bracket. The long lever arm with the small roller at its left-hand end is here clearly visible. The weight attached to theleft end of the lever arm to hold the roller in contact with the plane on which it rolls can also be seen.

forms the defining surface against which the crystal lamina is bent. The crystal is backed by a rubber gasket before the rear half of the crystal block is clamped on. Thus, only the convex face must be accurately lapped to an optical finish. At the end of the lapping procedure described in reference 13, the concave cast iron lap, which itself acquires a high optical polish, is set on an optical bench and examined optically by placing a line source of light at the center of curvature and observing its image with a microscope. A Hartman diagram of two zones reveals that the focus is approximately 0.016 mm. wide. This, then, indicates the degree of optical perfection attained by the convex crystal blocks.

The crystal laminae were cut from a single slab of quartz, which was ground flat and polished to approximately the final thickness prior to cutting.

The angle between the (310) crystal planes and the faces of the slab was determined on the two crystal spectrometer by replacing crystal B thereon with the slab (set for reflection of the beam from the above mentioned (310) planes) and locating the "parallel position". Crystal A was another quartz plate whose reflecting planes were also the (310) planes. The slab (whose orientation on the support bracket of the crystal B pivot was determined by a 3-point contact between the polished crystal surface and three ball bearings pressed tightly into shallow holes in the surface of the bracket) was then rotated 180° about an axis perpendicular to its face and the "parallel

position" was again located. The difference in the two "parallel position" readings is equal to twice the angle between the crystal planes and its faces. This angle was re-adjusted, by grinding, to the desired value α, and by keeping track of its direction, it was possible to clamp the crystals, when finished, correctly in the crystal blocks. (See page 9 for the requirement which fixes α.)

Special precautions were taken in lapping to prevent the development of surface stresses. Unnecessary heating in the lapping procedure was avoided. In the final stages of lapping, only the finest abrasive was used. The prolonged use of the fine abrasive made certain that no scratches were left from the coarser abrasive. Such scratches are invisible but can be revealed by etching the quartz. This is based on the theory that the scratches are actually grooves filled up with minute particles of quartz which can be removed by etching. The minute particles wedged in the grooves contribute to the surface stresses. Thus, if the two faces of a lamina are not scratched equally (which is usually the case), the etching process which relieves the strain will tend to make the lamina "curl" thus ruining the optical features of its faces. It is necessary to etch the crystals for two reasons: (1) to prevent breaking when being bent due to surface stresses, (2) to relieve the surface strains in order to be sure that the crystal planes are actually plane prior to bending.

The crystals used in the point-focusing monochromator were etched and found to be without a single scratch. Furthermore, they were examined on an optical flat before and after etching and no appreciable change was observed. The crystals are optically flat to within two fringes, the slight curvature tending to change the radius of the focal circle slightly.

PART V

EXPERIMENTAL RESULTS

Having obtained a focused beam by the procedures of Part IV, the problem is to find some appropriate sample for a scattering experiment. Since none of the improvements of beam intensity suggested in Part III were made at the date of writing this thesis, it was necessary to limit oneself to a relatively good scatterer. Two different samples of carbon black were picked out, one with average particle radius 54 Å (carbolac 1) and the other with radius 230 Å. The size and size distribution of the former was given by the manufacturer on the basis of electron microscope measurements and the latter was determined from the measurement of ninety particles photographed on the electron microscope in the Chemistry Division.

Carbon blacks, including the above, have been studied before[14,15,16], so that the present study does not reveal anything new regarding these samples. However, the purpose of the experiment was to check on the performance of the instrument and, particularly, on the luminosity of the direct beam. Since there exists no simple way to measure the direct beam intensity, the exposures required for satisfactory diffraction patterns from the carbon blacks are a good measure of the performance of the point focusing instrument.

The sample of carbon black was held in a ring 5 cm. in diameter and 0.4 cm. in axial thickness, with a 0.001" thick

nylon sheet glued to each side (to form a shallow cylindrical cavity which was packed full of the carbon). It was placed at a distance of 655 mm. from the point focus where the photographic plate was located. The irradiated volume was approximately 1.6 cm^3.

METHOD OF DETECTION

As has been previously mentioned, the scattered intensity was recorded on x-ray film, the direct beam being blocked out by means of a tungsten wire. See Plate 9.

After the diffraction pattern was obtained, it was necessary to measure the film density (and hence, the scattered intensity) versus the distance away from the center i.e. the scattering angle. This was done by means of a recording microphotometer. The light beam of the microphotometer was approximately the same elongated shape and size (0.89 mm. by 0.18 mm.) as the point focus and was oriented in the same way relative to the x-ray film. This light beam was allowed to scan the diffraction pattern along a diameter, the transmitted light being allowed to illuminate one junction of a thermopile which was connected to the coil of a d'Arsonval galvanometer, and the deflection of the latter being recorded photographically.

We have assumed that the following formula holds true, namely,

$$I_s = (1/kt) \log(x_o/\bar{x}) \qquad (68)$$

(a) Point Focus (Enlarged 5.8 times)
3 minute exposure at 20 PKV and 20 MA with beam in air.

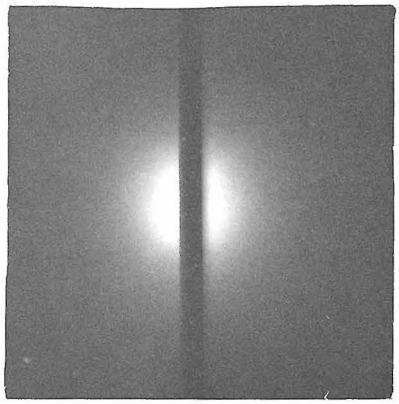

PLATE 9

(b) Diffraction Pattern of Carbon Black (Carbolac 1)
(Enlarged 5.8 times)
3 hours exposure at 35 PKV and 20 MA with beam in helium atmosphere. Average particle radius 54 Å.

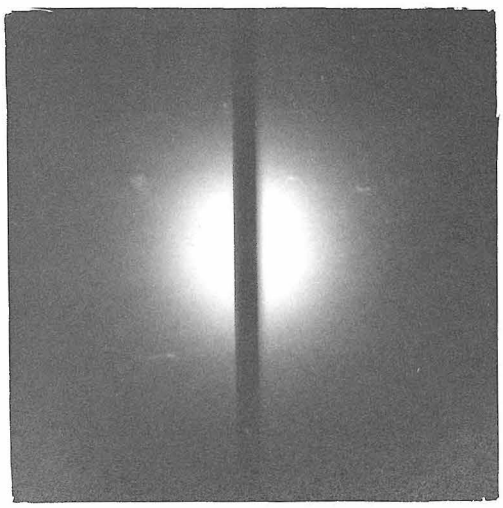

(c) Diffraction of Carbon Black (Enlarged 5.8 times)
3 hours exposure at 35 PKV and 20 MA with beam in helium atmosphere. Average particle radius 230 Å.

where I_s is the scattered x-ray intensity.

k is some constant dependent on the speed of the x-ray film.

t is the x-ray exposure time.

x_o is the maximum galvanometer deflection from totally dark film to clear film.

x is the galvanometer deflection from totally dark film to some exposed portion of the film.

This formula and its range of validity were verified experimentally.

In the case of small particles, theoretical curves for various types of particle size distributions have been worked out[4] and plotted in terms of log (I_s/I_o). It is easily seen that the coefficient of the logarithmic term above appears as an additive constant in such a plot and is, therefore, of little interest.

The microphotometer curve is treated in the following manner. It is placed over a sheet of ordinary graph paper and the values x are read off for various scattering angles on both sides of the maximum. The dark readings having been taken at the beginning and the end of the microphotometer run are connected by a straight line and used as a reference line from which x is measured. Although the thermopile drifts during the run due to increase in temperature, the value of x_o remains almost constant since both the light and dark readings are affected in the same way.

A commercially built microphotometer with beam size 0.01 mm. x 0.05 mm. was also used to analyze the diffraction

patterns but no appreciable difference was observed in the microphotometer runs of the two instruments. Microphotometer curves by the latter instrument for the two kinds of carbon blacks are shown in Figs. 9 and 10.

The ratio x_o/x is calculated and its logarithm is plotted versus the square of the scattering angle on log paper. Curves representing different exposures for a given sample are plotted on the same graph and are then compared with theoretical curves worked out by Roess and Shull[4]. The method of comparison is explained in the section that follows.

LOW ANGLE SCATTERING DUE TO SMALL PARTICLES

The above mentioned investigators have worked out the intensity curves for spherical particles with different types of size distributions, rectangular, Maxwellian and Gaussian. The Maxwellian type distributions seem to be the only applicable ones to our carbon blacks, see Fig. 11.

The theory upon which the above curves are based can be summarized in the following manner. The intensity scattered at a small angle ϵ by particles whose size distribution is M(R), R being the radius, is given by

$$I(\xi) = KI_e\rho_e^2\int_0^\infty M(R)R^3S(R,\xi)dR \qquad (69)$$

where

$$\xi = (2\pi/\lambda_0)\epsilon \qquad (70)$$

I_e is the Thomson scattering factor which is essentially constant for the small angles we shall consider. ρ_e is the electron density assumed uniform throughout the particle and $S(R,\xi)$ is the

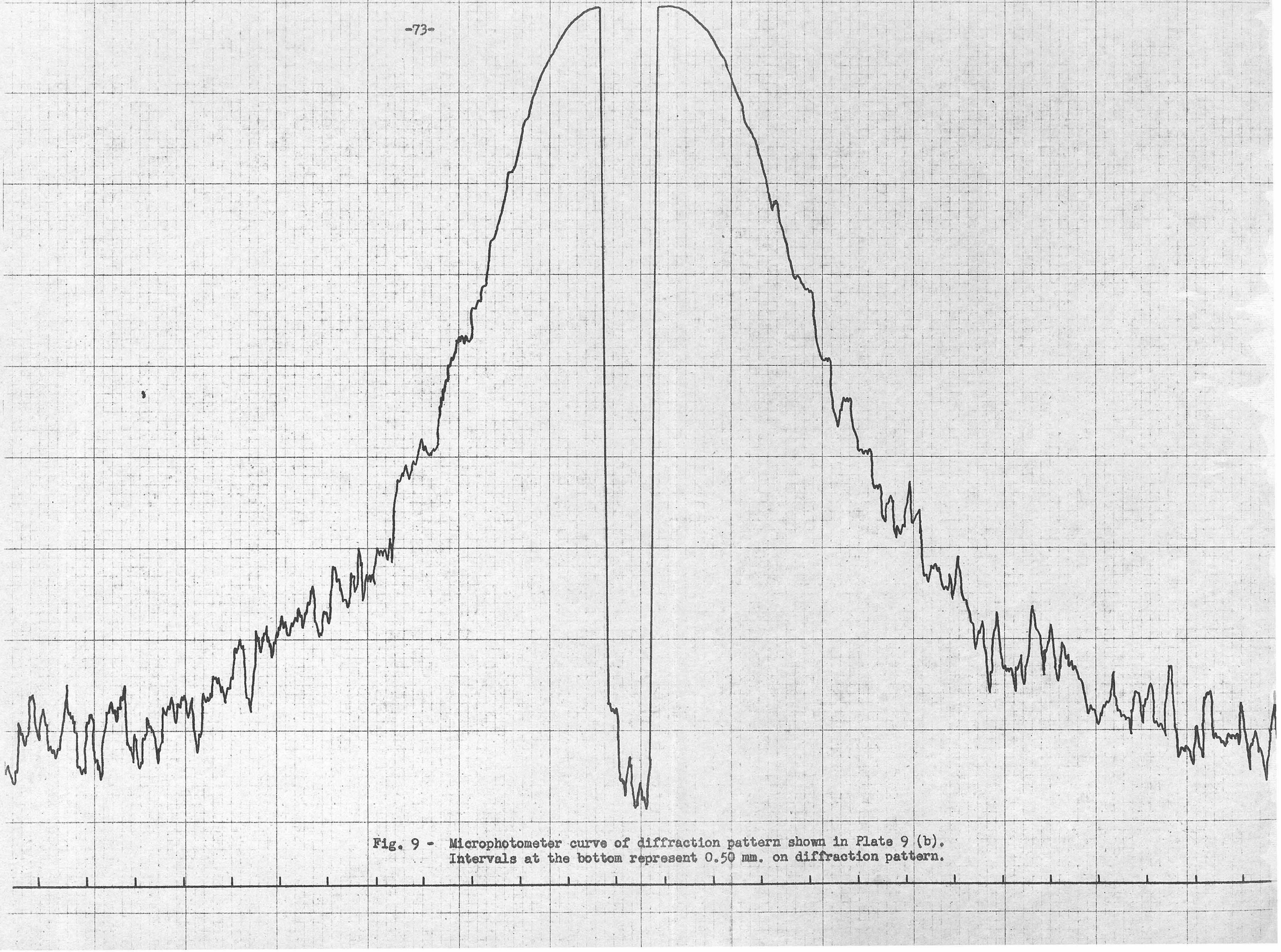

Fig. 9 - Microphotometer curve of diffraction pattern shown in Plate 9 (b).
Intervals at the bottom represent 0.50 mm. on diffraction pattern.

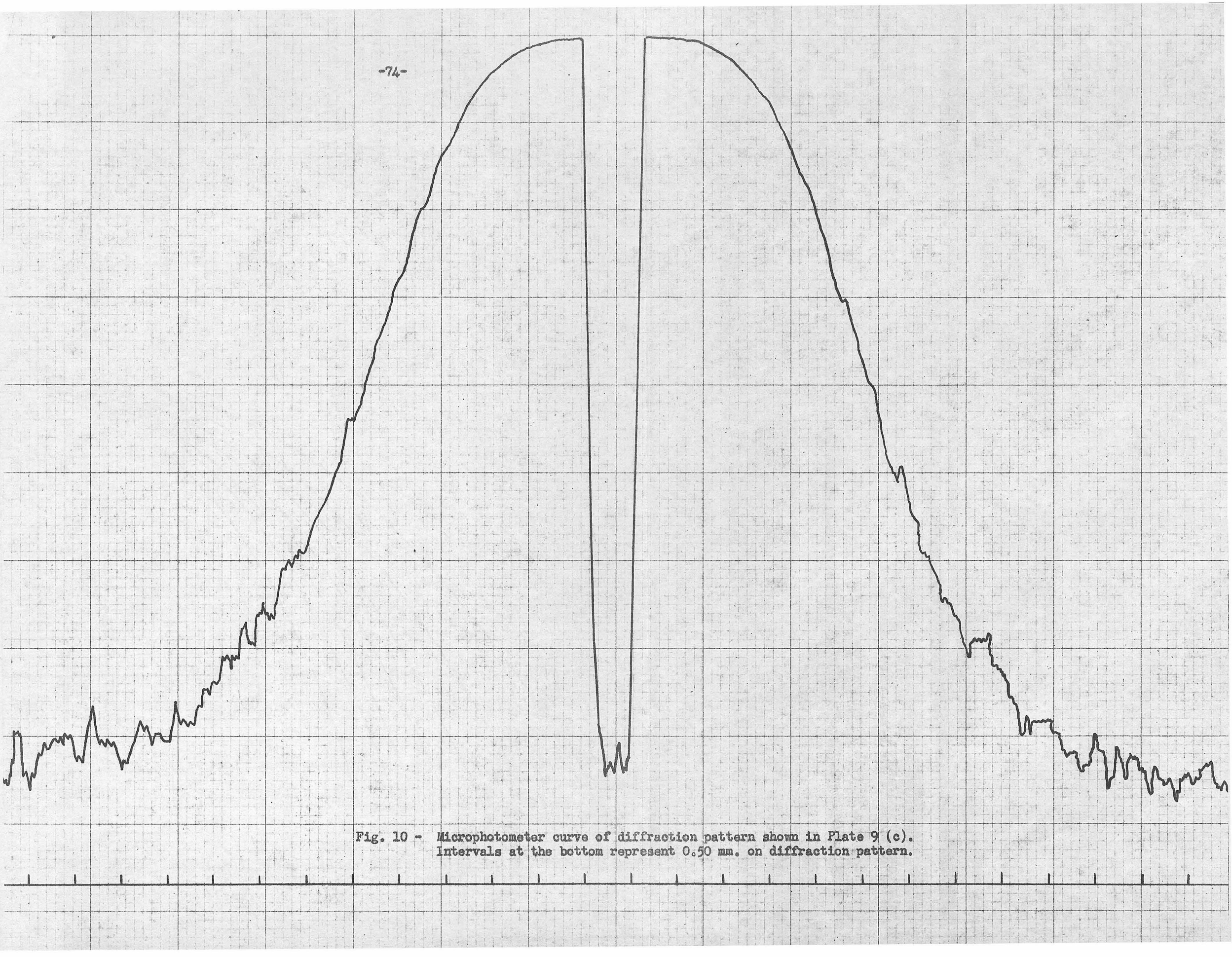

Fig. 10 - Microphotometer curve of diffraction pattern shown in Plate 9 (c).
Intervals at the bottom represent 0.50 mm. on diffraction pattern.

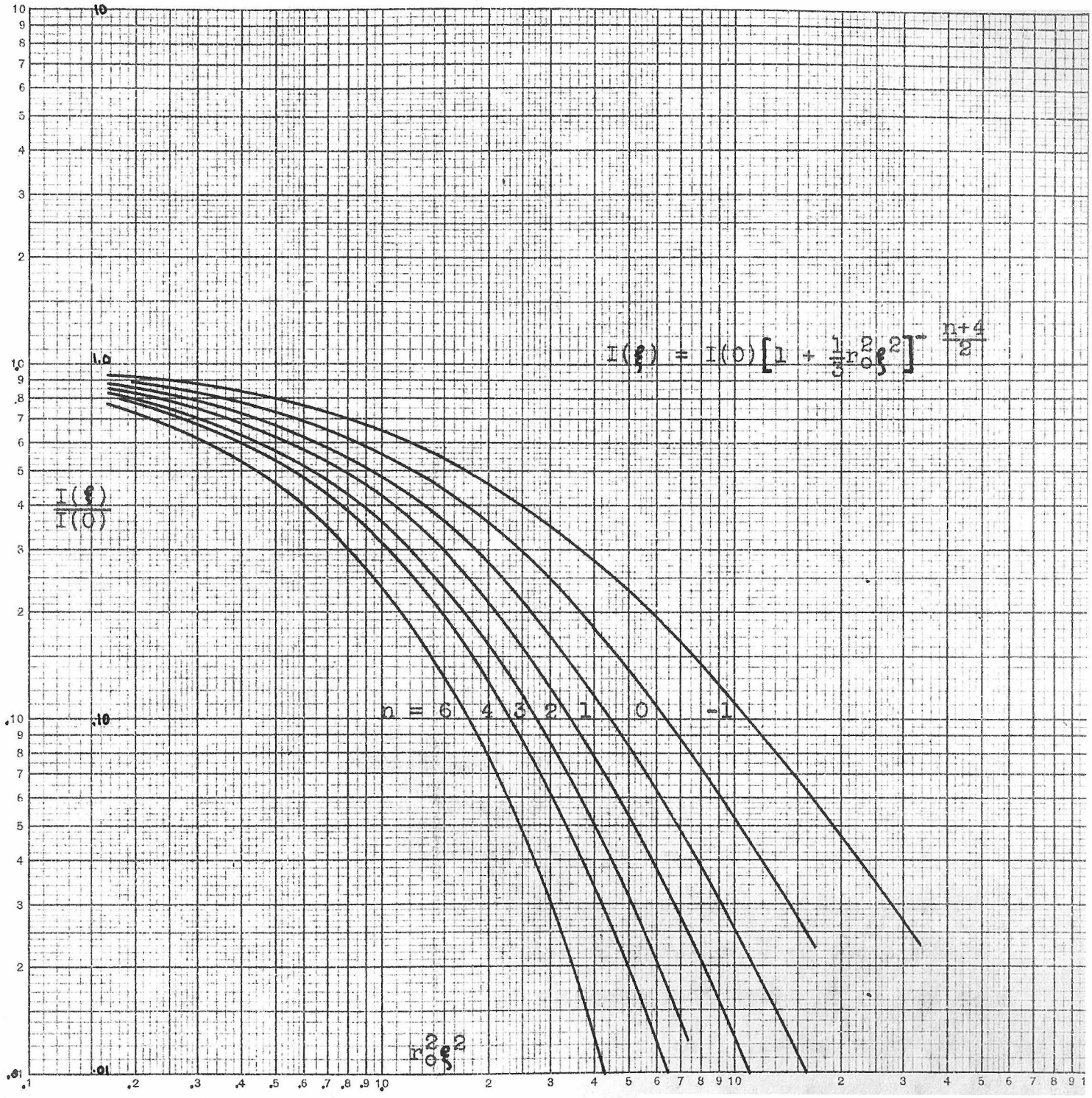

Fig. 11 - Angular dependence of scattered intensity for Maxwellian distribution of particle sizes.

scattering function characteristic of the particle size R and its geometrical shape. M(R)dR represents the total mass of particles in the size range R to R+dR. K is a constant proportional to the total mass.

For spherical particles Guinier[1] has shown that

$$S(R,\xi) = \exp(-r^2 \xi^2/3) \tag{71}$$

where he identifies r with the radius of gyration of the particle. For spheres

$$R = (5/3)^{\frac{1}{2}} r \tag{72}$$

The Maxwellian distribution function M, which we are interested in, can be expressed as a function of the radius of gyration and the parameters r_o and n as follows

$$M(r) = \frac{2}{r_o^{n+1} \Gamma(\frac{n+1}{2})} r^n \exp(-r^2/r_o^2) \tag{73}$$

Substituting eqs. (71) and (73) into (69) and integrating, we get

$$I(\xi) = I(0)\left[r_o^2 \xi^2/3 + 1\right]^{-(n+4)/2} \tag{74}$$

where I(0) is a complicated expression involving the parameters r_o and n and is of no interest here. Eq. (74) has been plotted, $\log I(\xi)/I(0)$ versus $\log r_o^2 \xi^2$, for several values of n.

Since we are interested in the average particle radius $\bar{R}$, we can define the average radius of gyration $\bar{r}$ as that radius which divides the mass distribution M(r) in two. This has been worked out[4] for several values of n, as follows:

n	0	1	2	3	4	5
$\bar{r}/r_o$	0.227	0.693	1.183	1.677	2.176	2.674

The experimental points are plotted $\log\log(x_o/x)$ versus $\log\xi^2$. By translating the experimental points horizontally and vertically until they match one of the theoretical curves, the value n is obtained immediately. If the horizontal shift of the experimental points relative to the theoretical curve is x units, this being obtained by dividing any reading on the abscissa of the latter by the corresponding reading on the abscissa of the former, then

$$\log x + \log\xi^2 = \log(r_o^2\xi^2)$$

and in view of eq. (70) the above reduces to

$$r_o = (\lambda_o/2\pi)x^{\frac{1}{2}} \tag{75}$$

To find the average particle radius, use is made of the above table and eqs. (72) and (75), thus

$$\bar{R} = (5x/3)^{\frac{1}{2}}(\bar{r}/r_o)(\lambda_o/2\pi) \tag{76}$$

where the ratio $\bar{r}/r_o$ must be chosen for the particular value of n found in matching the curves. The curves drawn through the experimental points are the best matching theoretical curves.

PARTICLE SIZE DETERMINATIONS OF CARBON BLACKS

The matching process described above has yielded the following results for the two kinds of carbon black. See Figs. 12 and 13.

Exposure Time	3 Hrs. in H_e Atmosphere	20 Hrs. in Air
Carbon Black	$n = 0$; $x = 40\times10^4$	$n = 1$; $x = 10\times10^4$
54 Å radius	$\bar{R} = 45.5$ Å	$\bar{R} = 69.4$ Å

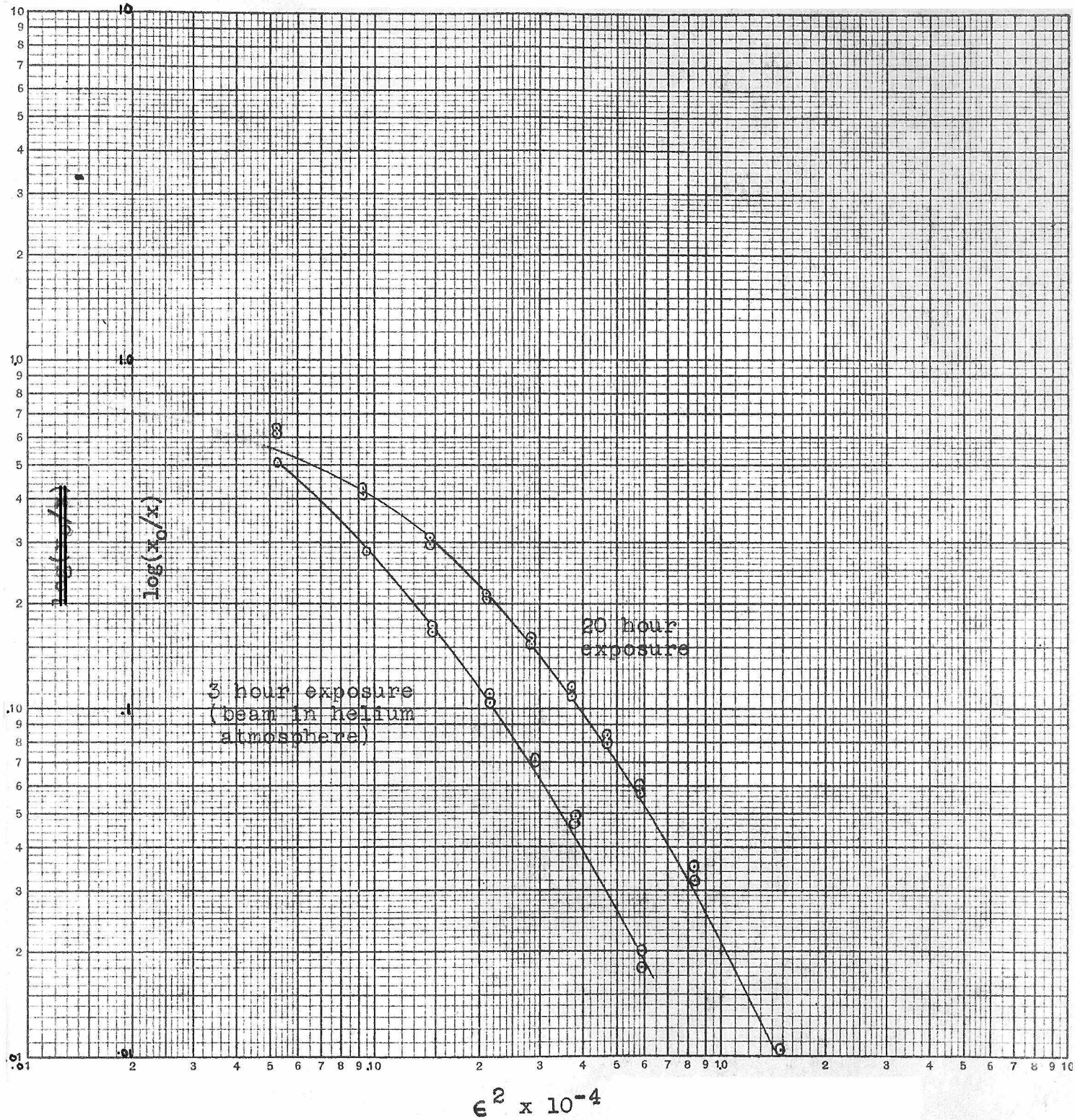

Fig. 12 - Carbon Black (Carbolac 1). Particle size - 54 Å radius.

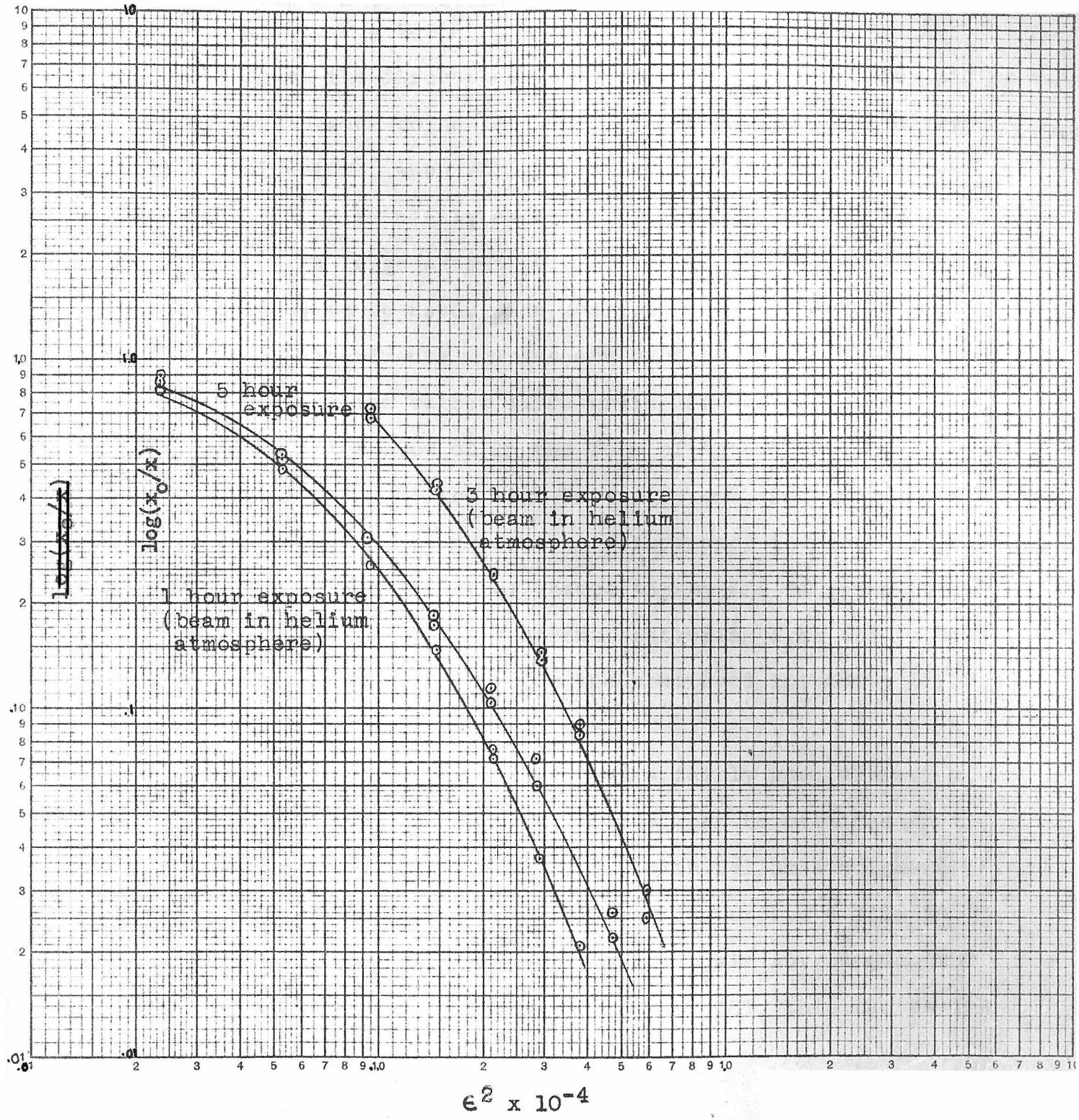

Fig. 13 - Carbon Black. Particle size - 230 Å radius.

Exposure Time	1 Hr. in H_e Atmosphere	5 Hrs. in Air	3 Hrs. in H_e Atmosphere
Carbon Black 230 Å radius	n=4; $x=14.5\times10^4$ $\overline{R}$ = 262 Å	n=3; $x=14\times10^4$ $\overline{R}$ = 197 Å	n=4; $x=17.4\times10^4$ $\overline{R}$ = 286 Å

Although the discrepancies in size determination for different exposures seem to be large at first sight, the actual experimental points, when shifted vertically to form one curve, fall in line quite nicely except for the end points which determine to a large extent the particular theoretical curve (and hence n) to be used. The end points on the low intensity side of the experimental curves are hard to determine with accuracy because of the rather large grain size of ordinary x-ray film. The grains show up in the form of "grass" on the microphotometer curve. At the high intensity end, and hence at very small scattering angles, the discrepency is probably due to either a slight amount of scattering by the tungsten wire (beam stop) or possibly incoherent scattering from the crystals, both of which may contribute to the scattered intensity at very low angles (i.e. ϵ = 0.0015 radians).

As one can see from the graphs, a fairly good exposure i.e. one that gives measurable results, can be obtained in 1 hour of exposure at 35PKV and 20 ma. with Helium atmosphere surrounding the beam. The direct beam can expose a film in about 15 seconds at 20PKV and 20 ma. with air surrounding the beam. With the changes mentioned in Part III, this can be improved considerably.

REFERENCES

(1) A. Guinier, Ann. de physique. (1939) 12, 161.

(2) R. S. Bear and O. E. A. Bolduan, J. App. Phys. (1951) 22, 191.

(3) R. von Nardroff, Phys. Rev. (1926) 28, 240.

(4) C. G. Shull and L. C. Roess, J. App. Phys. (1947) 18, 295.

(5) K. L. Yudowitch, J. App. Phys. (1949) 20, 174.
(1949) 20, 1232
(1951) 22, 214

(6) O. E. A. Bolduan and R. S. Bear, J. App. Phys. (1949) 20, 983.

(7) J. W. M. DuMond, R. S. I. (1950) 21, 188.

(8) Compton and Allison, "X-ray in Theory and Experiment" Van Nostrand Co., Inc., New York (1935).

(9) J. Johansson, Zeitschr. f. Phys. (1933) 82, 507.

(10) H. H. Johann, Zeitschr. f. Phys. (1931) 69, 185.

(11) J. E. White, J. App. Phys. (1950) 21, 855.

(12) E. Ingelstam, Arkiv. f. Mat., Astron. och Fysik (1939) 27B N:o 4.

(13) J. W. M. DuMond, D. A. Lind, E. R. Cohen, R. S. I. (1947), 18, 617.

(14) P. Krishnamurti, Ind. J. Phys. (1930) 5, 472.

(15) B. E. Warren, Phys. Rev. (1936) 49, 885.

(16) J. Biscoe and B. E. Warren, J. App. Phys. (1942) 13, 364-371.